UNIVERSITY OF CALIFORNIA
SANTA CRUZ

UNCONVENTIONAL PHASE TRANSITIONS IN DISORDERED AND INTERACTING SYSTEMS

A dissertation submitted in partial satisfaction of the
requirements for the degree of

DOCTOR OF PHILOSOPHY

in

PHYSICS

by

Shijun Sun

June 2024

The Dissertation of Shijun Sun
is approved:

Professor Arthur P. Ramirez, Chair

Professor Sergey Syzranov

Professor Josh Deutsch

Peter Biehl
Vice Provost and Dean of Graduate Studies

Table of Contents

List of Figures

List of Tables

Abstract

Unconventional phase transitions in disordered and interacting systems

by

Shijun Sun

This thesis will start by presenting an equivalence between a broad class of interacting disorder-free and disordered non-interacting systems. Such systems include, but are not limited to, nodal semimetals, dilute gases of bosons, trapped-ion systems with long-range interactions, and superconductive films. This equivalence is powerful: on the one hand, it allows one to simulate many-body effects by mapping them to single-body effects in disorder potentials; on the other hand, one can predict new types of phase transitions by mapping existing ones to them.

After establishing the equivalence, I will discuss three examples of such unconventional phase transitions found by duality mapping. For the first example, I will show that the BCS-BEC crossover can be mapped to a disorder-driven transition in nodal-point semimetal using the derived duality. For the second example, I will show that the BCS-superconducting transition can be mapped to a disorder-driven transition in nodal-line semimetals. These two disorder-driven transitions are different from the Anderson metal-insulator transition, which expands the types of disorder-driven transitions in non-interacting systems.

The third example is an unconventional interaction-driven transition found by mapping disorder-driven transitions to them. I will derive a phase transition of a dilute

gas of bosons with power-law dispersion at finite temperatures between a phase where the bosons are effectively non-interacting and a phase where the bosons are strongly interacting. I will also discuss an example spin model that exhibits this transition, which is the d-dimensional XXZ model with long-range interactions, with the interaction strength decaying as the distance to the power δ. The elementary excitations in this model are magnons with dispersion $k^{\delta-d}$ with attractive interactions. The spin model might be realized, and the phase transition can be detected in trapped-ion experiments.

Finally, in the last part of this thesis, I will discuss the effects of quenched disorder in magnetic materials. I will focus on a special type of quenched disorder — spin vacancies. Though the spin vacancies are defects achieved by substituting a non-magnetic ion to replace the original magnetic ion, the screening by the surrounding bulk spins can introduce a free-spin degree of freedom, a "quasispin", to the vacancies, which leads to a $1/T$ contribution to the magnetic susceptibility. I will derive this quasispin effect for Ising chains with nearest- and next-to-nearest-neighbor interactions. I will also study the effective interactions between the spin vacancies mediated through the bulk spins.

Acknowledgments

First of all, I would like to thank my advisor, Sergey Syzranov, for his guidance and constant support during my Ph.D. journey. Sergey has helped me tremendously in my development as a physicist. I have benefited a lot from his advices not only in physics, but also in scientific writing, presentation and networking skills.

I am grateful to Michael Dine, who was my advisor in my first 2.5 years of Ph.D. Michael is extremely knowledgeable and is very generous with his time and wisdom. As his student, I have developed a broader perspective on field theory and on particle physics in general. I still benefited from this broad perspective even after I moved to condensed matter physics.

I am also grateful to Aris Alexandradinata, Josh Deutsch, Arthur P. Ramirez, Sriram Shastry, and Edgar Shaghoulian for their helpful advice.

I have been fortunate throughout the years to share the friendship with amazing graduate students and postdocs: Omar Aguilar, Batoul Banihashemi, Runze Chi, Sri Aditya Gadam, Kejun Li, Pankaj Munbodh, Samantha Shears, Zijian Song, Pavlo Sukhachov, Zhencheng Wang, Siyu Zhu.

I would also like to thank my non-physicist friends, who I shared laughter and tears with: Xinyun Cui, Yanqing Liu & Pouya, Yannong He, Jack Li, Mali Peng, Gagandeep Sachdeva, Yufei Shan, Qiuxia Tang, Yuanqing Xue, Yan Zhang, Peng Zhou.

Last but not least, I am grateful to my parents for their support and love, without which I would not be able to finish my Ph.D.

Chapter 1

Introduction

Real materials always contain quenched disorder to some degree, therefore, idealized theoretical models that assume spatial homogeneity only give accurate predictions when the effects of disorders are unimportant. Here, by quenched disorder, I mean defects that are fixed and not evolving over time, e.g., vacancies, random fields, and bond defects. The opposite type of disorder, which is often referred to as "annealed disorder", are disorders that can slowly rearrange and equilibrate, e.g., defects in soft matter. This thesis focuses on the former type, quenched disorder.

Quenched disorder can lead to effects drastically different from the effects in clean systems. In 3 dimensions or higher, sufficiently strong disorder potentials can lead to the localization of the wavefunctions; this is known as the Anderson localization [1], which has no counterpart in clean systems. In magnetic materials, quenched disorders can lead to a different ground state of the system (e.g., random-field Ising model in 2D does not ferromagnetically order) and can introduce a new phase transition (e.g.,

spin-glass transition for systems with random-bond-disorders).

This chapter and the following three chapters will focus on a subset of disordered systems — disordered non-interacting electrons, where the disorder can be modeled by a random field coupled to the electrons. This can be described by the following Hamiltonian

$$\hat{H} = \hat{H}_0 + \hat{H}_1. \tag{1.1}$$

Here, $\hat{H}_0$ is the Hamiltonian of the clean system, and $\hat{H}_1$ is the coupling to the disorder potential. In general, $\hat{H}_1$ can be written as

$$\hat{H}_1 = u(\mathbf{r}) + \vec{\sigma} \cdot \vec{u}_s(\mathbf{r}) + \vec{\sigma} \cdot [\vec{u}_o(\mathbf{r}) \times \hat{\mathbf{p}}] \,,$$

where the first term is the coupling to a scalar disorder potential, which is analogous to a random shift to the chemical potential of the electron; the second term describes the interaction of the electron with a random magnetic field; and the last term describes the spin-orbit coupling with a disorder potential. From now on, I will focus on the potential for scalar disorder; the other two cases can be analyzed using a similar treatment.

Because the scalar disorder potential is equivalent to a random shift of the chemical potential, one can always shift the chemical potential such that the disorder potential has zero mean $\langle u(\mathbf{r}) \rangle_{\text{dis}} = 0$. In this thesis, I consider Gaussian distributed random potential (i.e., only correlations between two disorder potentials is nonzero, $\langle u(\mathbf{r}) u(\mathbf{r'}) \rangle_{\text{dis}} \neq 0$, and correlations involve three or more disorder potentials can be neglected).

Physical quantities that are most interesting to us are often the so-called self-averaged quantities. For these quantities, the experimentally measured values are their

disorder averaged values $\left\langle \hat{\mathcal{O}} \right\rangle_{\text{dis}}$ which depend only on the mean and the correlation between the disorder potentials. This is because, for a sufficiently large system, i.e., system size much larger than the correlation length, one can imagine dividing the system into regions of size correlation length and averaging over the values of the observable in different regions. This gives the disorder-averaged value. Theoretically, these disorder-averaged values can be computed diagrammatically or by using a field-theoretical description. In what immediately follows, I will discuss a field-theoretical description for non-interacting systems with quenched disorder.

1.1 Field theoretic description

In clean systems, thermodynamic quantities can be computed by differentiating the free energy with respect to the conjugate variable, for example, the density of quasiparticles can be computed by

$$\langle \hat{n} \rangle = \frac{\partial}{\partial \mu} \left(k_B T \log Z \right), \tag{1.2}$$

where Z is the partition function, and μ is the chemical potential. In order to derive the disorder-averaged quantities, one needs to compute disorder averages for the logarithm of the partition function $\langle \log Z \rangle_{\text{dis}}$. For example, the disorder-averaged particle density is given by

$$\langle \hat{n} \rangle_{\text{dis}} = k_B T \frac{\partial}{\partial \mu} \langle \log Z \rangle_{\text{dis}} . \tag{1.3}$$

In general, disorder averages for the logarithm of the partition function are hard to compute. However, there are three known methods for computing disorder-averaged

quantities:

1. Replica trick [2, 3], which is based on the following formula

$$\log Z = \lim_{R\to 0} \frac{Z^R - 1}{R}. \tag{1.4}$$

   Using this method, one can now compute an easier quantity $\left\langle Z^R \right\rangle_{\text{dis}}$ for integer-valued R and take the formal limit of $R \to 0$ to extrapolate $\langle \log Z \rangle_{\text{dis}}$.

   This method can be used to describe interacting systems, but it is not as rigorous as the other two methods.

2. Supersymmetry method [4, 5]: since Bosonic and Fermionic determinants cancel

$$\mathcal{Z}_\zeta = \int \mathcal{D}\psi e^{-\int \bar{\psi} M \psi} = \det(M)^{-\zeta}, \quad \begin{cases} \zeta = 1 & \text{for bosons} \\ \zeta = -1 & \text{for fermions} \end{cases} \tag{1.5}$$

   one can introduce both Bosonic and Fermionic degrees of freedom to the partition function to ensure the partition function is unity $\mathcal{Z}_{\text{SUSY}} = \mathcal{Z}_{\zeta=-1}\mathcal{Z}_{\zeta=+1} \equiv 1$. The supersymmetry method is mathematically rigorous, but it only applies to non-interacting systems.

3. Keldysh formalism [6, 7, 8]: includes a forward and a backward time contour, which cancels with each other and the partition function $\mathcal{Z} \equiv 1$.

   The Keldysh formalism can treat interactions and non-equilibrium, but it is the hardest-to-use method among the three.

In this thesis, I will use the Replica method to write field theories for disordered systems. The partition function for a disordered metal described by the Hamiltonian Eq. (1.1)

can be written as

$$\left\langle Z^R \right\rangle_{\rm dis} = \int \mathcal{D}u\mathcal{D}\Psi\mathcal{D}\Psi^\dagger \exp\Bigg[-\int \psi_a^\dagger \left(E - \hat{h}_{\rm dis} + u(\mathbf{r}) \right) \psi_a \, d^d\mathbf{r} \\ -\frac{1}{2}\int u(\mathbf{r})\, U^{-1}(\mathbf{r}-\mathbf{r}')\, u(\mathbf{r}')\, d^d\mathbf{r} d^d\mathbf{r}' \Bigg], \tag{1.6}$$

where a is the replica index, Ψ is a R-component vector, and we consider Gaussian distributed disorder potential with correlation $\langle u(\mathbf{r})u(\mathbf{r}')\rangle_{\rm dis} = U(\mathbf{r}-\mathbf{r}')$. Here, we used the Einstein summation convention, i.e., repeated index is summed over. Carrying out the integration over the disorder potential in the above equation gives

$$\left\langle Z^R \right\rangle_{\rm dis} = \int \mathcal{D}u\mathcal{D}\Psi\mathcal{D}\Psi^\dagger \exp\Bigg[-\int \psi_a^\dagger \left(E - \hat{h}_{\rm dis} + u(\mathbf{r}) \right) \psi_a \, d^d\mathbf{r} \\ +\frac{1}{2}\int \psi_a^\dagger(\mathbf{r})\psi_b^\dagger(\mathbf{r}')\, U(\mathbf{r}-\mathbf{r}')\, \psi_b(\mathbf{r}')\psi_a(\mathbf{r})\, d^d\mathbf{r} d^d\mathbf{r}' \Bigg]. \tag{1.7}$$

We see here that averaging disorder leads to an effective attractive interaction among the particle fields.

1.2 Anderson localization

Non-interacting disordered systems can undergo a disorder-driven phase transition — the Anderson metal-insulator transition. In 3-spatial dimensions or higher, for a sufficiently strong disorder, the wavefunctions of electrons in the disorder potential can become localized

$$|\psi(r)| \sim \exp\left(-\frac{|r-r_0|}{L_c} \right), \tag{1.8}$$

where L_c is the localization length. Therefore, in the localized phase, the electric conductivity approaches zero, and the system becomes an insulator. This phenomenon

was introduced by Phillip Anderson in 1958 [1] and has been extensively studied ever since [9, 10, 11, 12]. For systems in one or two spatial dimensions, localization happens with an arbitrarily weak disorder [13, 14, 15, 16].

The precursor of the Anderson localization is the so-called weak localization, this effect can be intuitively understood from quantum interferences between paths of electrons. When computing the quantum mechanical probability of getting from one point to another, one sum over the complex amplitudes of all paths connecting the two points. Typically, the phase differences between different paths are large, and the interference between paths is unimportant. However, for a self-intersecting path, e.g., the path shown in Fig. 1.1a, there always exists a corresponding non-intersecting path with the same length and with the opposite direction of the trajectory along the loop, e.g., Fig. 1.1b. The amplitudes of these two paths have the same phase and are enhanced by quantum interference.

$$|A_1 + A_2|^2 = 4|A_1|^2 \tag{1.9}$$

Here, A_1 and A_2 are the amplitudes of the paths shown in Fig. 1.1a and b. We see from here that the total probability is twice as large as the classical probability without interference. This interference increases the scattering rate and therefore, decreases conductivity. In one- and two-dimension, the probability of having path intersections is unity, regardless of the strength of the disorder. On the contrary, in three-dimension, the probability of path intersection is less than unity, therefore, a sufficiently strong disorder is needed for localization.

In the following sub-section, I will introduce a more rigorous description of

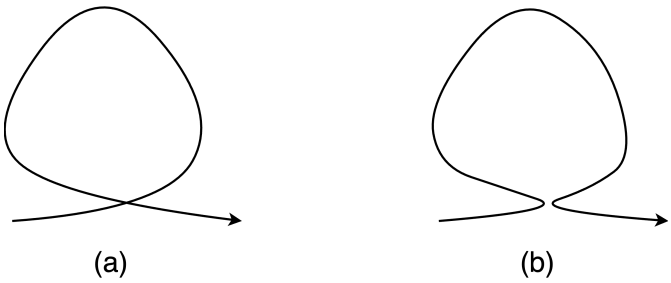

Figure 1.1: (a) Self-intersecting path; (b) Path with the same length as (a), but with an opposite travel direction along the loop.

the behavior of disordered electronic systems. I will derive the non-linear sigma model (NLσM) for a disordered system, which describes the long-wavelength behavior of the system. The Anderson localization transition can be derived from a renormalization group (RG) analysis of the NLσM.

1.2.1 Sigma model

In this section, I will derive the NLσM for the orthogonal symmetry class (class AI in the Cartan symbol) explicitly. The NLσM of other symmetry classes can be derived similarly. Systems in the orthogonal symmetry group have time-reversal symmetry T with $T^2 = +1$, and no charge-conjugation symmetry nor chiral symmetry, as shown in Table. 1.1. This corresponds to, e.g., spinless particles with time-reversal symmetry. With time-reversal symmetry, the disordered Hamiltonian is invariant under the following transformation

$$T: \quad \hat{h}_{\rm dis} \to U_T \, \hat{h}_{\rm dis}^T \, U_T^{-1} \tag{1.10}$$

where U_T is a unitary transformation. Therefore, for spinless particles, the Hamiltonian satisfies

$$\hat{h}_{\rm dis} = \hat{h}_{\rm dis}^T. \tag{1.11}$$

For spinful particles, e.g., for spin-1/2, the Hamiltonian satisfies

$$\hat{h}_{\rm dis} = \hat{\sigma}_y \, \hat{h}_{\rm dis}^T \, \hat{\sigma}_y \tag{1.12}$$

where $\hat{\sigma}_y$ is the Pauli-y matrix in the spin space.

With the time-reversal symmetry, it is natural to write the particle fields in Eq. (1.7) in terms of Nambu spinors

$$\Phi_a = \sqrt{\mathcal{N}} \begin{pmatrix} \psi_a \\ \\ \bar{\psi}_a^T \end{pmatrix} \quad \text{and} \quad \bar{\Phi}_a = (C\Phi_a)^T = \sqrt{\mathcal{N}} \left(\bar{\psi}_a, \psi_a^T \right), \tag{1.13}$$

where $\mathcal{N}$ is a normalization factor, and $C = \tau_x$ with τ_x being the Pauli-x matrix in the Nambu space. Here, I assumed that the particles are spinless. For spinful particles, the operator C can have structures in the spin space.

In terms of the Nambu spinors, the field-theoretical action can be written as

$$S = \frac{1}{2} \int_{\mathbf{r}} \bar{\Phi}_a(\mathbf{r}) \begin{pmatrix} E - \hat{h} & 0 \\ \\ 0 & E - \hat{h} \end{pmatrix} \Phi_a(\mathbf{r}) - g \int_{\mathbf{r}} \bar{\Phi}_a \Phi_a \bar{\Phi}_b \Phi_b \tag{1.14}$$

Here, we used that $\hat{h}^T = \hat{h}$ since the Hamiltonian is spinless and time-reversal invariant; and we consider short-range correlated disorder with strength $g = \int_{\mathbf{r}'} U(\mathbf{r} - \mathbf{r}')$. To describe physical quantities that contain both retarded and advanced Green's functions, for example, $\left\langle G^A(E) G^R(E') \right\rangle_{dis}$, one considers field-theoretical actions with structures

in both retarded and advanced spaces, which can be written as follows

$$S = \frac{1}{2}\int_{\mathbf{r}} \bar{\Phi}(\mathbf{r})\left(E - \frac{\varepsilon}{2} - \hat{h}\right)\Phi(\mathbf{r}) + \frac{\varepsilon}{4}\int_{\mathbf{r}} \bar{\Phi}\Lambda\Phi - g\int_{\mathbf{r}} \bar{\Phi}_a\Phi_a\bar{\Phi}_b\Phi_b \tag{1.15}$$

where Φ is a $4R$-dimensional vector, with the first $2R$ components in the retarded space and the latter $2R$ components in the advanced space; Λ is a $4R \times 4R$ matrix, $\Lambda = \mathrm{diag}\{I_{\mathrm{Nambu,replica}}, -I_{\mathrm{Nambu,replica}}\}$, where $I_{\mathrm{Nambu,replica}}$ is a $2R\times 2R$ identity matrix; and $\varepsilon = E - E'$.

One can now decouple the quartic term in both the Cooper and the diffusion channel using a matrix-valued field. This brings the action to the following form

$$S = \frac{1}{2}\int_{\mathbf{r}} \bar{\Phi}(\mathbf{r})\left[\left(E - \frac{\varepsilon}{2}\right) + \frac{\varepsilon}{2}\Lambda - \hat{h}\right]\Phi(\mathbf{r}) + \frac{\pi\nu g}{4}\int_{\mathbf{r}} \bar{\Phi}_a Q_{ab}\Phi_b + \frac{(\pi\nu)^2 g}{4}\int_{\mathbf{r}} Q^2. \tag{1.16}$$

Integrating out Φ in the above action gives

$$S = \int_{\mathbf{r}}\left[-\frac{1}{2}\mathrm{Tr}\log\left(-\hat{\xi} + \frac{\varepsilon}{2}\Lambda + \frac{\pi\nu g}{2}Q\right) + \frac{g(\pi\nu)^2}{4}\mathrm{Tr}Q^2\right]. \tag{1.17}$$

Here, $\hat{\xi} = \hat{H} - E - \frac{\varepsilon}{2}$. The saddle point equation for the Q matrix is given by

$$Q = \frac{1}{\pi\nu}\int \frac{d^d p}{(2\pi)^d}\left(-\hat{\xi} + \frac{\varepsilon}{2}\Lambda + \frac{\pi\nu g}{2}Q\right)^{-1}. \tag{1.18}$$

Solving the saddle point equation in the limit of small ε leads to $Q = U^\dagger\Lambda U$, where $U^\dagger U = 1$.

The saddle point equation has a $Sp(4R)$ symmetry. To see this, let us consider a transformation $\mathcal{G}$ to the Nambu spinor

$$\Phi \to \mathcal{G}\Phi, \quad \text{where} \quad \mathcal{G}^T\tau_x\mathcal{G} = \tau_x. \tag{1.19}$$

Then, the transformation leaves the action invariant. A symmetry transformation preserves τ_x belongs to the Sp group, so $\mathcal{G} \in Sp(2_\tau \times 2_{RA} \times R)$. A solution of the saddle

point equation is invariant under the subgroup $Sp(2_\tau \times R) \times Sp(2_\tau \times R)$. Therefore, the NL$\sigma$M lives in the group manifold $\frac{Sp(4R)}{Sp(2R)\times Sp(2R)}$. The group manifold for the NLσM of other symmetry classes can be derived similarly and are summarized in Table. 1.1.

For systems with a finite Fermi surface, we can expand around the Fermi surface and the operator $\hat{\xi} \approx v_F \mathbf{n} \cdot \nabla$. Expanding the $\mathrm{Tr}\log(\cdots)$ to the lowest non-vanishing order in ε and ∇, one gets the effective action for the Goldstone modes [5, 17]

$$S = \int_{\mathbf{r}} \mathrm{tr}\left[\frac{v_F^2}{g}\left(\partial_\mu Q\right)^2 - \frac{i\pi\nu}{4}\varepsilon\Lambda Q\right]. \tag{1.20}$$

The localization effect can be derived from an RG analysis of the conductivity in dimensions close to two, $d = 2 + \epsilon$. Since the derivation is standard and is not the main focus of this thesis, I will not derive the RG equation here, but only provide the result. The renormalization of the conductivity obeys the equation [5, 17, 18]

$$\partial_\ell g = -(d-2)g + \frac{2}{\pi}g^2 \tag{1.21}$$

under a rescaling of length scales by a factor of e^ℓ. Therefore, disordered systems in the orthogonal class always localize in two dimensions. The results of the RG analysis for disordered systems in all ten symmetry classes are summarized in Table. 1.1.

1.3 Unconventional disorder-driven phase transitions

It has been commonly believed that the Anderson metal-insulator transition is the only disorder-driven transition in non-interacting disordered systems. However, pioneer works [19, 20, 21, 22, 23, 24, 25] have shown that a broad class of systems can display disorder-driven transitions distinct from Anderson localization. Such systems

are non-interacting disordered systems with power-law quasiparticle dispersion $\xi_{\mathbf{k}} = a|\mathbf{k}|^{\alpha}$, in spatial dimensions higher than 2α. These systems include 3-dimensional Dirac and Weyl semimetals, cold-atom systems with long-range interactions, etc. The phase transition manifests itself in the disorder-averaged density of states (DoS), conductivity, and other observables [24, 25, 26, 27, 28, 29, 30, 31, 32, 33, 34, 35].

In this section, I will briefly review this unconventional disorder-driven transition, which was extensively studied in Refs. [24, 25, 28] (see also Ref. [19] for a review). I will first review the RG analysis of disordered non-interacting systems with power-law dispersion and derive the phase transition (Sec. 1.3.1). Then, I will discuss the critical behavior of the observables near the transition (Sec. 1.3.2).

1.3.1 Renormalization group analysis

The disorder potentials are chosen to be short-range correlated with a coupling constant κ characterizing the strength of the disorder

The renormalization of the disorder strength involves repeatedly integrating out shells of momenta

$$Ke^{-l} < |\mathbf{k}| < K, \tag{1.22}$$

$$\left\langle U(\mathbf{r})U(\mathbf{r}')\right\rangle_{\text{dis}} = \kappa\delta\left(\mathbf{r}-\mathbf{r}'\right). \tag{1.23}$$

where K is the ultraviolet cutoff and $l > 0$. The parameters in the original theory get renormalized, and the renormalized values "flow" under RG with respect to different length scales (i.e., they are functions of l). We can then ask how the coupling constants flow as one goes to long wavelengths (large l). The RG flow is most interesting if it

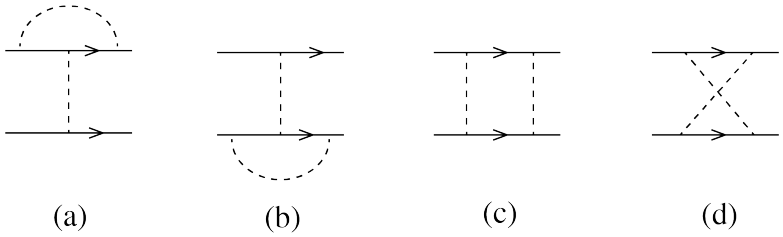

Figure 1.2: Diagrams for the renormalization of the disorder strength at one-loop order.

develops an unstable fixed point at a certain value of the coupling constant, such value is usually referred to as the "critical value". If this happens, the behavior of the system is drastically different if the coupling constant is smaller or larger than the critical value, as the RG flows to different regions at long wavelengths. Therefore, the unstable fixed point distinguishes two different phases of the theory and describes a phase transition.

The diagrams that contribute to the renormalization of the disorder strength are shown in Fig. 1.2. Evaluating these diagrams at zero external frequencies and momenta, we get the renormalization of the disorder strength given by

$$\delta\kappa = 4\kappa^2 \int_{Ke^{-l}<|\mathbf{k}|<K} \frac{d^d k}{(2\pi)^d} \frac{1}{\xi_{\mathbf{k}}^2} = \frac{4\kappa^2 S_d K^{d-2\alpha}}{a^2(2\pi)^d} \frac{1-e^{-(d-2\alpha)l}}{d-2\alpha}, \tag{1.24}$$

where S_d is the area of a d-dimensional unit sphere. Differentiating with respect to l, one can derive the RG equation for the disorder strength

$$\partial_l \kappa = 4\kappa^2 \frac{S_d K^{d-2\alpha}}{a^2(2\pi)^d}. \tag{1.25}$$

It is convenient to define a dimensionless coupling constant

$$\gamma = 4\kappa \frac{S_d K^{d-2\alpha}}{a^2(2\pi)^d}. \tag{1.26}$$

Then, the RG equation for the dimensionless coupling constant is

$$\partial_l \gamma = -(d-2\alpha)\gamma + \gamma^2. \tag{1.27}$$

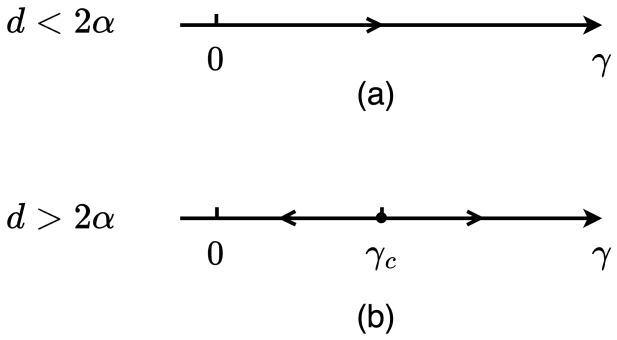

Figure 1.3: The RG flow of Eq. (1.27). In high dimensions, $d > 2\alpha$, the unstable fixed point at $\gamma_c = d-2\alpha$ describes a phase transition between an effective disorder-free phase and a strongly disordered phase. This disorder-driven phase transition is different from the Anderson localization transition.

The RG flow of the dimensionless coupling constant in Fig. 1.3 follows directly from this equation, where the arrow pointing to the direction of the change of γ as l increases. One can see from Fig. 1.3 that, in high dimensions, $d > 2\alpha$, the RG flow has an unstable fixed point at $\gamma_c = d - 2\alpha$. For $\gamma < \gamma_c$, the RG flows to the Gaussian fixed point at $\gamma = 0$ at long distances. This corresponds to a phase effectively disorder-free. For $\gamma > \gamma_c$, the RG flows to large γ and the system is strongly disordered at long distances. Therefore, the fixed point at γ_c describes a disorder-driven phase transition. One can also compute the critical exponent from the RG equations, for example, the correlation length exponent $\nu = \frac{1}{d-2\alpha}$ and the dynamical exponent $z = \alpha + \frac{d-2\alpha}{4}$ [24, 25, 28]. These critical exponents are different from the critical exponents of the Anderson metal-insulator transitions. Therefore, the transition reviewed in this section belongs to a universality class different from the universality classes of the Anderson transitions.

1.3.2 Critical behavior in density of states

Physical observables exhibit singular behavior near the non-Anderson disorder-driven transition at $\gamma = \gamma_c$. For example, the disorder-averaged DoS takes the following form near the critical point [19, 24, 25, 28]

$$\rho(E,\kappa) = (E - E_{\rm c})^{\frac{d}{z}-1}\, \Phi\left[(\kappa - \kappa_{\rm c})\,/\,(E - E_{\rm c})^{\frac{1}{z\nu}}\right] + \rho_{\rm smooth}\ , \tag{1.28}$$

where z and ν are the dynamical exponent and the correlation length exponent, respectively; Φ is a universal scaling function. Near the critical disorder strength, the DoS $\rho \propto |E - E_c|^{\frac{d-z}{z}} + \rho_{\rm smooth}$. For strong disorder, $\kappa > \kappa_c$, the DoS is roughly a constant for low energies, and scales like $\rho \propto (\kappa - \kappa_c)^{(d-z)\nu} + \rho_{\rm smooth}$. And for weak disorder, $\kappa < \kappa_c$, the DoS scales similarly as in a disorder-free system, $\rho \propto (\kappa_c - \kappa)^{-d\nu\left(\frac{z}{\alpha}-1\right)} |E - E_c|^{\frac{d-\alpha}{\alpha}}$, and increases rapidly as the disorder strength approaches to the critical value.

	T	C	S	Compact NLσM manifold	RG of σ	Examples of systems
A	0	0	0	$\frac{U(2N)}{U(N)\times U(N)}$	WL	Integer quantum Hall, Diffusive metal
AI	1	0	0	$\frac{Sp(4N)}{Sp(2N)\times Sp(2N)}$	WL	Diffusive metal
AII	-1	0	0	$\frac{O(2N)}{O(N)\times O(N)}$	WAL	Quantum spin Hall, $\mathbb{Z}_2$ topological insulator, Diffusive metal + spin-orbit coupling
AIII	0	1	0	$U(N)$	$\equiv 0$	Bipartite hopping + random flux
BDI	1	1	1	$\frac{U(2N)}{Sp(2N)}$	$\equiv 0$	Bipartite hopping
CII	-1	1	-1	$\frac{U(N)}{O(N)}$	$\equiv 0$	Bipartite hopping
D	0	0	1	$\frac{O(2N)}{U(N)}$	WAL	2D $p_x + ip_y$-wave superconductor
C	0	0	-1	$\frac{Sp(2N)}{U(N)}$	WL	Singlet superconductor in $\vec{B}$, Quantum spin Hall
DIII	-1	1	1	$O(N)$	WAL	Superconductor + spin-orbit coupling
CI	1	1	-1	$Sp(2N)$	WL	Singlet superconductor

Table 1.1: Table of Altland-Zirnbauer symmetry classes. The first column is the ten symmetry classes in Cartan symbols. T, C, and $S = TC$ in the 2nd, 3rd, and 4th column are the time-reversal, particle-hole, and chiral symmetries. 0 denotes the absence of the symmetry; 1 (-1) denotes the presence of the symmetry and operating the symmetry transformation twice gives $+1$ (-1). A disordered system belonging to a specific symmetry class can be described by an effective NLσM whose group manifold is listed in the 5th column. Here, N denotes the number of replicas. The RG of the conductivity in these NLσM are given in the 6th column. Here, "WL" denotes weak localization of the disordered system, "WAL" denotes weak anti-localization of the disordered system, and "$\equiv 0$" means the renormalization of the conductivity vanishes.

Chapter 2

Interaction-disorder duality

The previous chapter has made clear that the Anderson metal-insulator transition is not the only phase transition in non-interacting disordered systems. This chapter and the following chapter focus on expanding the types of disorder-driven phase transitions that are different from the Anderson localization transition. The new disorder-driven transitions are predicted using the previously well-studied phase transitions in interacting clean systems via a duality that we will derive in this chapter. This chapter is based on Ref. [36].

The duality maps an interacting system in d spatial dimensions with a low DoS at the chemical potential to a disordered non-interacting system in $d+1$ spatial dimensions. In addition to predicting new disorder-driven transitions, such duality mapping also allows for easier simulation of manybody effects in the interacting system, by mapping them to single particle properties in the disordered system.

In what follows, I will first give a heuristic argument for why we may expect

interacting disorder-free systems to behave similarly to disordered non-interacting systems and when we can expect them to be equivalent systems in Sec. 2.2. I will then summarize the duality mapping we derived in Ref. [36] (Sec. 2.1) and provide an explicit derivation for a correspondence of observables on both sides to all orders in perturbation theory (Sec. 2.3). Finally, I will give an example of such equivalent systems — a quantum dot and a one-dimensional disordered wire in Sec. 2.4.

2.1 Summary of the mapping

The duality maps a d-dimensional interacting system to a $d+1$-dimensional disordered non-interacting system. The interacting system is described by a Hamiltonian of the form

$$\hat{H} = \int \hat{\Psi}^\dagger(\mathbf{r})\, \xi_{\hat{\mathbf{p}}} \hat{\Psi}(\mathbf{r})\, d^d\mathbf{r} - \frac{1}{2}\int \hat{\Psi}^\dagger(\mathbf{r})\hat{\Psi}^\dagger(\mathbf{r}')U(\mathbf{r}-\mathbf{r}')\hat{\Psi}(\mathbf{r}')\hat{\Psi}(\mathbf{r})\, d^d\mathbf{r} d^d\mathbf{r}'. \tag{2.1}$$

Here, $\hat{\Psi}^\dagger$ is the particle creation operator; $\xi_{\hat{\mathbf{p}}}$ is the single-particle dispersion; and $U(\mathbf{r}-\mathbf{r}')$ is the interaction potential. The particles may be bosonic or fermionic. The dispersion $\xi_{\hat{\mathbf{p}}}$ and the interaction can either be scalar functions of the momenta and positions, describing spinless particles, or matrices in band and spin spaces, describing particles with non-trivial band and spin structures.

The mapping applies to a subset of interacting systems satisfying the following constraint. The screening effects of the interaction potential are either suppressed or have no qualitative effects on the observables and phenomena of interest. Examples of systems where screening effects are suppressed are systems with low density of states

at the chemical potential, such as nodal semimetals and dilute gases with the power-law dispersion $\xi_{\mathbf{p}} \propto p^{\alpha}$ in dimensions $d > \alpha$. This includes graphene, Weyl/Dirac semimetals in $d = 2$ and $d = 3$, parabolic semimetals in $d = 3$, and dilute Bose and Fermi gases in dimension $d > \alpha$. We will discuss this constraint in more detail and the example systems that the mapping applies in the following sections.

The dual disordered system is $d + 1$-dimensional, with the extra dimension mapped to the Matsubara time dimension in the interacting system. The disordered system has an additional pseudospin-1/2 structure for reasons that will become clear in the following section.

The disordered system that is mapped to an attractive interacting system is described by the Hamiltonian

$$\hat{h} = \hat{\sigma}_z \xi_{\hat{\mathbf{p}}} + \hat{\sigma}_y p_{d+1} + \hat{\sigma}_z u(\boldsymbol{\rho}), \tag{2.2}$$

where $\hat{\sigma}_x$, $\hat{\sigma}_y$ and $\hat{\sigma}_z$ are the Pauli matrices in the pseudospin-1/2 space, p_{d+1} is the component of momentum along the $d+1$-st dimension, which is mapped to the Matsubara time direction in the interacting system; and $u(\boldsymbol{\rho})$ is the disorder potential.

We do not assume a specific form of interaction in the interacting system. The form of interaction is mapped to a corresponding form of disorder correlation $\langle u(\boldsymbol{\rho}) u(\boldsymbol{\rho}') \rangle_{\text{dis}} = U(\mathbf{r} - \mathbf{r}') \delta(\mathrm{r}_{d+1}, \mathrm{r}'_{d+1})$. For example, short-range interaction that is described by a coupling constant g is mapped to short-range correlated disorder potential with the disorder strength characterized by the same coupling constant

$$g = \int U(\mathbf{r} - \mathbf{r}') d^d \mathbf{r}' = \int \left\langle u(\boldsymbol{\rho}) u(\boldsymbol{\rho}') \right\rangle_{\text{dis}} d^{d+1} \boldsymbol{\rho}'. \tag{2.3}$$

The disordered system that is mapped to a repulsive interacting system is described by the Hamiltonian

$$\hat{h}_{\text{repulsive}} = \hat{\sigma}_z \xi_{\hat{\mathbf{p}}} + \hat{\sigma}_y p_{d+1} + \hat{\sigma}_y u(\boldsymbol{\rho}), \tag{2.4}$$

with the only difference compared to Eq. (2.2) being a Pauli-y matrix multiplied by the disorder potential rather than the Pauli-z matrix.

The duality mapping holds at the operator level. As we will show in Sec. 2.3, each observable in the interacting system corresponds to a disorder-averaged quantity in the disordered system, whose values are the same, to all orders in perturbation theory. For example, the number density operator $\hat{n} = \hat{\Psi}^\dagger(\mathbf{r})\hat{\Psi}(\mathbf{r})$ in the interacting system is mapped to the following disorder-averaged quantity in the dual disordered system

$$\hat{\rho}_s(\boldsymbol{\rho}) = \frac{1}{4} \operatorname{Tr}\left[\hat{\sigma}_z G^R(\boldsymbol{\rho}, \boldsymbol{\rho}, 0) + \hat{\sigma}_z G^A(\boldsymbol{\rho}, \boldsymbol{\rho}, 0)\right], \tag{2.5}$$

	Interacting model	Disordered model
Coordinates	$(\tau, \mathbf{r})$	$(\mathrm{r}_{d+1}, \mathbf{r})$
Temperature/size	T	$1/\ell_{d+1}$
Particle types/ boundary conditions	Boson/Fermion	Periodic/anti-periodic boundary conditions along $d+1$ direction
Interaction potential/ disorder correlation	$U(\mathbf{r}-\mathbf{r}')$	$\langle u(\mathrm{r}_{d+1}, \mathbf{r}) u(\mathrm{r}_{d+1}, \mathbf{r}')\rangle_{\text{dis}}$
Observables	$\hat{n}$ (density)	$\hat{\rho}_s$, Eq. (2.5)

Table 2.1: Correspondence between quantities in the interacting disorder-free and non-interacting disordered systems.

where Tr is taken over the pseudospin degree of freedom, and $G^R(\boldsymbol{\rho}, \boldsymbol{\rho}, E)$ and $G^A(\boldsymbol{\rho}, \boldsymbol{\rho}, E)$ are the retarded and advanced Green's functions.

The duality mapping is summarized in Table. 2.1.

2.2 Heuristic argument

To see the similarity between an interacting system and a disordered non-interacting system, let's start with the d-dimensional interacting system described by the Hamiltonian Eq. (2.1). The partition function of this interacting system can be written as

$$Z = \int \mathcal{D}\Psi\mathcal{D}\Psi^\dagger \exp\Bigg[- \int \Psi^\dagger \left(\partial_\tau + \xi_{\hat{\mathbf{p}}}\right) \Psi \, d\tau d^d\mathbf{r} + \frac{1}{2}\int \Psi^\dagger(\mathbf{r})\Psi^\dagger(\mathbf{r}')U(\mathbf{r}-\mathbf{r}')\Psi(\mathbf{r}')\Psi(\mathbf{r}) \, d\tau d^d\mathbf{r} d^d\mathbf{r}' \Bigg]. \tag{2.6}$$

For attractive interactions, one may introduce an auxiliary scalar field $\phi(\tau, \mathbf{r})$ to decouple the interaction term. This is the Hubbard-Stratonovich (HS) transformation. Then, the partition function can be written as

$$Z = \int \mathcal{D}\phi\mathcal{D}\Psi\mathcal{D}\Psi^\dagger \exp\Bigg[- \int \Psi^\dagger \left(\partial_\tau + \xi_{\hat{\mathbf{p}}} + \phi\right) \Psi \, d\tau d^d\mathbf{r} - \frac{1}{2}\int \phi(\tau,\mathbf{r})U^{-1}(\mathbf{r}-\mathbf{r}')\phi(\tau,\mathbf{r}') \, d\tau d^d\mathbf{r} d^d\mathbf{r}' \Bigg]. \tag{2.7}$$

One can see that the partition functions (2.6) and (2.7) are equivalent by integrating the HS field in Eq. (2.7). The transformed partition function has a nicer form than the original one because it is quadratic in the field Ψ.

Equation (2.7) has a similar form as a partition function of a disordered system,

with the path integral of the HS field ϕ interpreted by an average over disorder potentials, and the correlations between the disorder potentials are described by $U(\mathbf{r}-\mathbf{r}')$. However, there are important differences between these two similar-looking partition functions. To make it explicit, let us integrate the particle fields Ψ in Eq. (2.7).

$$Z = \int \mathcal{D}\phi \, \det\left(\partial_\tau + \xi_{\hat{\mathbf{p}}} + \phi\right) \, \exp\left[-\frac{1}{2}\int \phi(\tau,\mathbf{r}) U^{-1}(\mathbf{r}-\mathbf{r}')\phi(\tau,\mathbf{r}')\, d\tau d^d\mathbf{r} d^d\mathbf{r}'\right] \quad (2.8)$$

Here, the determinant is produced from the Gaussian integration of the particle fields, which gives correction to the effective action of the field ϕ. Physically, this is due to the particles screening the interaction potential.

On the other hand, as we recall from Sec. 1.1, a field-theoretical description of disordered systems has additional structures in the replica, supersymmetry, or the Keldysh space, to ensure the partition function $Z = 1$. Consequently, the determinant in Eq. (2.8) is equal to one. In the replica method, this is because the limit of the number of replicas approaches zero. In supersymmetry representation, this is because the contributions from the bosonic and fermionic sectors cancel. Physically, this result can be phrased as the disordered potentials are not screened in systems with quenched disorder.

Therefore, the claim of our mapping is that a subset of interacting systems where the screening effects are either suppressed or have no qualitative effects on the observables of interest can be mapped to disordered non-interacting systems. The screening effects are suppressed in systems with low DoS at the chemical potential. For example, in nodal semimetals and dilute gases with the power-law dispersion $\xi_{\mathbf{p}} \propto p^\alpha$ in dimensions $d > \alpha$, the DoS is proportional to $\rho(E) \propto E^{\frac{d}{\alpha}-1} \to 0$ for $E \to 0$, the

effect of screening is proportional to the DoS and is suppressed. Such systems include graphene, Weyl/Dirac semimetals in $d = 2$ and $d = 3$, parabolic semimetals in $d = 3$, and dilute Bose and Fermi gases in dimension $d > \alpha$.

In addition, the duality mapping can also apply to systems with finite DoS, so long as the phenomena of interest are unaffected by screening. An example is the BCS superconducting transition in 2D metals. Near the phase transition, the dominant effects are from the Copper channel, and the effects of screening are subdominant. Therefore, the duality mapping can be applied and map the BCS transition in 2D metals to a disorder-driven transition in 3D nodal-line semimetals. We will discuss this example in more detail in Sec. 3.2.

2.2.1 Matsubara time & Hermitization procedure

Another important difference between interacting and disordered systems is that, in contrast to interacting systems, disordered systems do not have the Matsubara time direction. As we recall from Sec. 1.1, the partition function of disordered systems Eq. (1.6) is defined at a specific energy E of the physical process, and the integral involves only spatial directions.

Therefore, the duality maps a d-dimensional interacting system to a $d+1$-dimensional disordered system, with the extra spatial dimension mapped to the Matsubara time direction. It is tempting to write the dual disordered Hamiltonian as

$$\hat{h}' = \partial_{d+1} + \xi_{\mathbf{p}} + u(\boldsymbol{\rho}), \tag{2.9}$$

where $\boldsymbol{\rho} = (\mathbf{r}, r_{d+1})$ is a $d+1$-dimensional vector, and $i\partial_{d+1} = i\frac{\partial}{\partial r_{d+1}}$ is the momentum

along the $d+1$-st dimension. This Hamiltonian matches with the Hamiltonian for interacting system Eq. (2.1). However, Eq. (2.9) is non-Hermitioan, with the first term anti-Hermitian and the latter two terms Hermitian.

The Hermitian Hamiltonian for the dual disordered system Eq. (2.2) is derived by applying a "Hermitization" procedure [37, 38, 39, 40] to the non-Hermitian Hamiltonian Eq. (2.9). The Hermitization procedure is as follows:

1. Any non-Hermitian Hamiltonian can be separated into a Hermitian part and an anti-Hermitian part and can be written as

$$\mathcal{H}_{\mathrm{NH}} = \mathcal{H}' + i\mathcal{H}'', \tag{2.10}$$

   with both $\mathcal{H}'$ and $\mathcal{H}''$ being Hermitian;

2. Then, one can double the Hilbert space and write an equivalent Hermitian Hamiltonian as follows

$$\mathcal{H}_{\mathrm{Hermitian}} = \hat{\sigma}_x \mathcal{H}' - \hat{\sigma}_y \mathcal{H}'', \tag{2.11}$$

   where σ_x and σ_y are the Pauli matrices. Please see the subsection 2.2.1.1 for an explanation of the equivalence between Eqs. (2.10) and (2.11).

Using the Hermitization procedure, we arrive at the Hamiltonian for the disordered system that is dual to the attractively interacting system, $\hat{h} = -\hat{\sigma}_y p_{d+1} + \hat{\sigma}_x \xi_{\hat{\mathbf{p}}} + \hat{\sigma}_x u(\boldsymbol{\rho})$, which matches Eq. (2.2) up to a rotation in the pseudospin basis.

2.2.1.1 More on the Hermitization procedure

We can understand the Hermitization procedure as follows. For non-Hermitian Hamiltonians, the energies of the states are complex numbers, and the left and right eigenstates are different and are given by

$$\mathcal{H}_{\mathrm{NH}} \left|\phi_R\right\rangle = E \left|\phi_R\right\rangle, \quad \mathcal{H}_{\mathrm{NH}} \left|\phi_L\right\rangle = E^* \left|\phi_L\right\rangle. \tag{2.12}$$

One can write a Hermitian Hamiltonian in a doubled Hilbert space as follows

$$\mathcal{H}_{\mathrm{Hermitian}} = \begin{pmatrix} 0 & \mathcal{H}_{\mathrm{NH}} - E \\ \mathcal{H}_{\mathrm{NH}}^{\dagger} - E^* & 0 \end{pmatrix} \tag{2.13}$$

Then, the states $\left(\left|\phi_R\right\rangle, 0\right)^T$ and $\left(0, \left|\phi_L\right\rangle\right)^T$ are the zero modes of this Hermitian Hamiltonian. For the zero-energy states of the original non-Hermitian Hamiltonian, $E = 0$, and the Hermitized Hamiltonian takes the form Eq. (2.11). These zero-energy states are the states we focus on in this chapter.

In summary, the non-Hermitian Hamiltonian Eq. (2.10) is equivalent to the Hermitian Hamiltonian Eq. (2.11) if we consider only the zero-energy states on both sides.

2.2.2 Mapping for repulsive interactions

The HS transformation we described in Eq. (2.7) applies only to attractive interactions. For repulsive interactions, the HS transformation can still be applied using an imaginary HS field. The partition function after the transformation is given

by

$$Z = \int \mathcal{D}\phi\mathcal{D}\Psi\mathcal{D}\Psi^{\dagger} \exp\Big[- \int \Psi^{\dagger} \left(\partial_{\tau} + \xi_{\hat{\mathbf{p}}} + i\phi\right) \Psi \, d\tau d^{d}\mathbf{r} \\ - \frac{1}{2} \int \phi(\tau, \mathbf{r}) \left[-U^{-1}(\mathbf{r} - \mathbf{r}')\right] \phi(\tau, \mathbf{r}') \, d\tau d^{d}\mathbf{r} d^{d}\mathbf{r}' \Big]. \qquad (2.14)$$

Note that the interaction potential $U(\mathbf{r} - \mathbf{r}') < 0$ for repulsive interactions. Therefore, the path integral of the HS field ϕ has the correct form as a Gaussian integral.

The partition function Eq. (2.14) resembles a partition function of a disordered system with an imaginary disorder potential. Mapping to an imaginary disorder potential is not as bizarre as it seems. Using the Hermitization procedure described in the previous section, we derive the Hamiltonian for the dual disordered system.

$$\hat{h}_{\text{repulsive}} = \hat{\sigma}_z \xi_{\hat{\mathbf{p}}} + \hat{\sigma}_y p_{d+1} + \hat{\sigma}_y u(\boldsymbol{\rho}) \qquad (2.15)$$

Here, we "Hermitize" the disorder potential by multiplying it with the Pauli matrix $\hat{\sigma}_y$ rather than $\hat{\sigma}_z$ as in the Hamiltonian Eq. (2.2) of disordered systems dual to attractively interacting systems.

2.3 Derivation of observable correspondence to all orders in perturbation theory

In this section, I provide a rigorous derivation of the duality to all orders in perturbation theory. The elements of the diagrammatic technique for the interacting disorder-free system and the disordered non-interacting system follow directly from the Hamiltonians Eqs. (2.1) and (2.2), and are shown in Fig. 2.1.

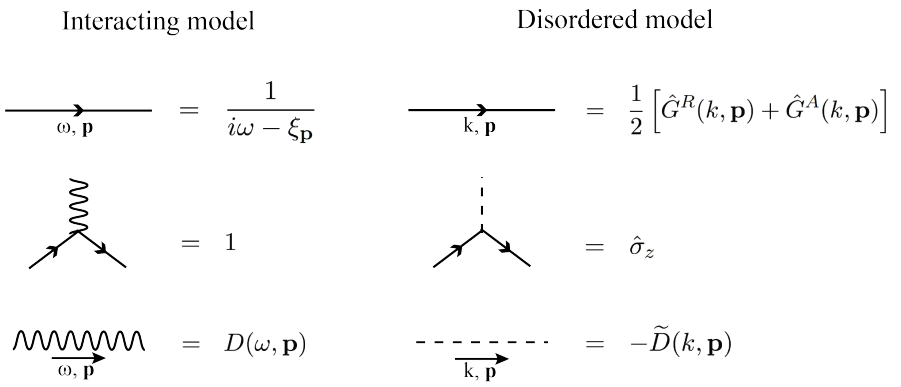

Figure 2.1: Elements of the diagrammatic technique for the interacting disorder-free (left) and non-interacting disordered (right) models in momentum space that illustrate perturbative equivalence between the two classes of systems. $D(\omega, \mathbf{p})$ and $-\widetilde{D}(k, \mathbf{p})$ are the interaction propagators and disorder lines, respectively. In the case of short-range interactions, both the interaction propagators and the impurity lines are independent of their frequencies and momenta and are described by the coupling constant defined above, $D(\Omega_i, \mathbf{P}_i) = \widetilde{D}(K_i, \mathbf{P}_i) = -g$.

The duality allows for a one-to-one mapping between operators in the interacting system and operators in the corresponding disordered system. An example of such operator mapping is the number-density operator $\hat{n} = \hat{\Psi}^\dagger(\mathbf{r})\hat{\Psi}(\mathbf{r})$ in the interacting system and the disorder-averaged quantity Eq. (2.5)

$$\hat{\rho}_s(\boldsymbol{\rho}) = \frac{1}{4}\,\mathrm{Tr}\left[\hat{\sigma}_z G^R(\boldsymbol{\rho}, \boldsymbol{\rho}, 0) + \hat{\sigma}_z G^A(\boldsymbol{\rho}, \boldsymbol{\rho}, 0)\right], \tag{2.5}$$

in the corresponding disordered system. The diagrams that contribute to the number-density operator are shown in Fig. 2.2a-c, while the diagrams for the disordered system that contribute to the disordered quantity Eq. (2.5) are shown in Fig. 2.2d. Example diagrams in the interacting system that can be neglected are shown in Fig. 2.2b,c. The diagrams in Fig. 2.2b involve polarization operators, i.e., parts of the diagram involve additional particle loops in between interaction propagators. These are the aforementioned diagrams that contribute to the screening effects. The polarization

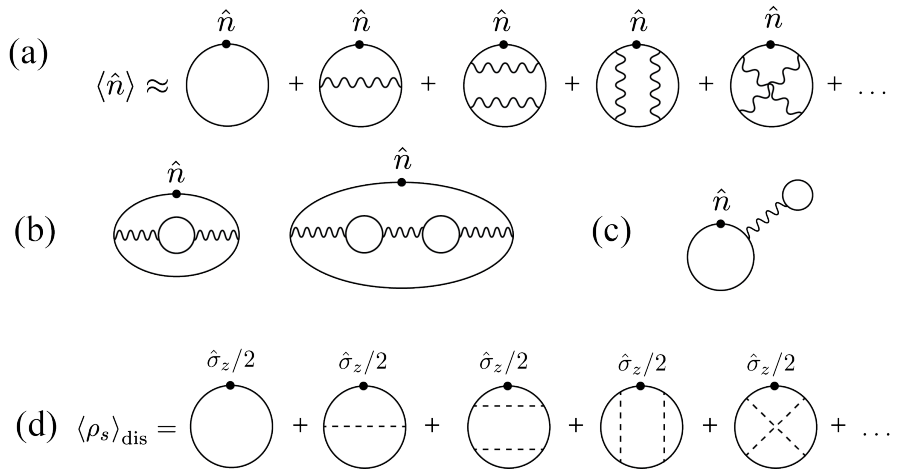

Figure 2.2: Diagrams for observables in interacting disorder-free systems and the corresponding non-interacting disordered systems. (a) Contributions to the number density of interacting particles. (b)-(c) Examples of neglected contributions; diagrams in (b) are neglected due to the suppression of screening effects; (c) is the Hartree contribution, which can be absorbed into a redefinition of the chemical potential. (d) Contributions to the corresponding disorder-averaged quantity ρ_s, given by Eq. (2.5).

operators are proportional to the DoS at the chemical potential of the system.

Therefore, for systems with low DoS at the chemical potential or phenomena whose screening effects are unimportant, diagrams in Fig. 2.2b can be neglected. The diagram in Fig. 2.2c is the Hartree contribution, whose effect can be absorbed in a redefinition of the chemical potential.

The remaining diagrams that contribute to the number-density operator in the interacting system are shown in Fig. 2.2a. Each of these remaining diagrams corresponds to a diagram for the dual disordered system, which are shown in Fig. 2.2d. Corresponding diagrams are diagrams that are identical to each other by replacing the interaction propagators with the disordered lines (dashed lines) and vice versa. The

diagrammatic correspondence holds to all orders in perturbation theory.

In what immediately follows, I will demonstrate that the values of the corresponding diagrams in the interacting and disordered systems match. I will first show this for short-range interaction and short-range correlated disorder potential. The interaction strength and the disorder strength match and are described by the same coupling constant

$$g = \int U(\mathbf{r} - \mathbf{r}')d^d\mathbf{r}' = \int \left\langle u(\boldsymbol{\rho})u(\boldsymbol{\rho}')\right\rangle_{\text{dis}} d^{d+1}\boldsymbol{\rho}'. \tag{2.16}$$

However, the mapping is not limited to short-range interaction and disorder correlation. In the next subsection, I will show a rigorous derivation of the mapping for general forms of the interaction and disorder correlation.

For short-range interactions, the value of a diagram with N interaction propagators contributing to the density of particles in the interacting system is given by

$$\pm\frac{g^N T^{N+1}}{V^{N+1}} \sum_{\omega,\mathbf{p}} \frac{1}{(i\omega_1 - \xi_{\mathbf{p}_1})^2} \frac{1}{i\omega_2 - \xi_{\mathbf{p}_2}} \cdots \frac{1}{i\omega_{2N} - \xi_{\mathbf{p}_{2N}}}. \tag{2.17}$$

Here, the "+" and "−" signs correspond to bosonic and fermionic particles, respectively; g is the coupling constant; T and V are the temperature and volume of the system; and the sum is carried over $N+1$ independent frequencies and momenta.

Each sum with respect to Matsubara frequencies ω in Eq. (2.17) can be replaced with two summations: $\sum_\omega \ldots = \frac{1}{2}\sum_\omega \ldots + \frac{1}{2}\sum_{-\omega} \ldots$, and (2.17) can be rewritten as

$$\pm\frac{g^N T^{N+1}}{2V^{N+1}} \sum_{\sigma=\pm1} \sum_{\omega,\mathbf{p}} \frac{1}{(i\omega_1\sigma - \xi_{\mathbf{p}_1})^2} \frac{1}{i\omega_2\sigma - \xi_{\mathbf{p}_2}} \cdots \frac{1}{i\omega_{2N}\sigma - \xi_{\mathbf{p}_{2N}}}. \tag{2.18}$$

The value of the corresponding diagram in the disordered system contributing to the

dual disorder-averaged quantity ρ_s with N disordered lines is given by

$$\pm\frac{g^N}{2V^{N+1}\ell_{d+1}^{N+1}}\sum_{\mathbf{p},k}\mathrm{Tr}\left[\frac{1}{ik_1\hat{\sigma}_x-\xi_{\mathbf{p}_1}\mathbb{1}_{2\times2}}\frac{1}{ik_1\hat{\sigma}_x-\xi_{\mathbf{p}_1}\mathbb{1}_{2\times2}}\cdots\frac{1}{ik_{2N}\hat{\sigma}_x-\xi_{\mathbf{p}_{2N}}\mathbb{1}_{2\times2}}\right], \tag{2.19}$$

where the "+" and "−" signs correspond to periodic and anti-periodic boundary conditions along the $d+1$-st dimension, respectively; g is the coupling constant that describes the strength of short-range correlated disorder potential; the dual disordered system has a volume of $V\ell_{d+1}$; the trace $\mathrm{Tr}\,[\ldots]$ is taken over the pseudospin degrees of freedom; and $\mathbb{1}_{2\times2}$ is the 2×2 identity matrix in the pseudospin space.

The value (2.18) of the diagram for the interacting disorder-free system matches the value (2.19) of the corresponding diagram for the non-interacting disordered system. This is because

1. The trace over the pseudospin space can be replaced by the summation of σ in Eq. (2.18). Since all the propagators in the square bracket in Eq. (2.19) commute with each other in the pseudospin space, one can replace the operator $\hat{\sigma}_x$ with its eigenvalues $\sigma_x=\pm1$ in the denominators.

2. The momentum summation of k in Eq. (2.19) is identical to the frequency summation ω in Eq. (2.18), because the temperature T of the interacting system matches the inverse length ℓ_{d+1} (cf. Table 2.1) and (fermionic) bosonic particles in the interacting system are mapped to (anti-)periodic boundary conditions in the disordered system.

In the subsection that immediately follows, I will provide a rigorous derivation

of the duality mapping without assuming a specific form of the interaction potential and the disorder correlation.

2.3.1 Derivation for a general form of interaction

In this section, I provide the derivation of the duality for a generic finite-range interaction and disorder correlation. The interaction propagator and the "impurity line" [41] are given by

$$D(\mathbf{r},\tau;\mathbf{r}',\tau') = -\left\langle T_\tau \hat{\phi}(\mathbf{r},\tau)\hat{\phi}(\mathbf{r}',\tau')\right\rangle = U(\mathbf{r}-\mathbf{r}'), \tag{2.20}$$

where $\hat{\phi}$ are the bosonic fields corresponding to the interaction between the particles, and

$$-\widetilde{D}(\boldsymbol{\rho}-\boldsymbol{\rho}') = \left\langle u(\boldsymbol{\rho})u(\boldsymbol{\rho}')\right\rangle_{\text{dis}} = U(\mathbf{r}-\mathbf{r}')\delta(r_{d+1}-r'_{d+1}). \tag{2.21}$$

Here, in accordance with the common convention, the impurity line (cf. Fig. 2.1) is defined to be positive for a real random potential. Note that the disorder correlation in the dual system is chosen to match the form of the corresponding interaction potential. The elements of the diagrammatic technique for both systems are shown in Fig. 2.1.

The value of each diagram with N interaction propagators contributing to the density of particles $\hat{n}$ in the interacting system is given by

$$(-1)^{N+F}\frac{T^{N+1}}{V^{N+1}}\sum_{\omega,\mathbf{p}}\frac{1}{(i\omega_1-\xi_{\mathbf{p}_1})^2}\frac{1}{i\omega_2-\xi_{\mathbf{p}_2}}\cdots\frac{1}{i\omega_{2N}-\xi_{\mathbf{p}_{2N}}}D(\Omega_1,\mathbf{p}_1)\ldots D(\Omega_N,\mathbf{p}_N). \tag{2.22}$$

Here, $F=1$ for fermionic particles and $F=0$ for bosonic particles; $D(\Omega_i,\mathbf{p}_i)$ is the interaction propagator in the frequency and momentum space, and the sum is carried

over $N+1$ independent frequencies and momenta, with the rest frequencies and momenta for the particle and interaction propagators determined by energy and momentum conservation laws. We assume the convergence of the sum for each diagram.

The bosonic propagator $D(\Omega_i, \mathbf{p}_i)$ is an even function of the Matsubara frequency Ω_i,. Therefore, each summation with respect to Matsubara frequencies ω in Eq. (2.22) can again be replaced with two summations with respect to ω and $-\omega$, $\sum_\omega \ldots = \frac{1}{2}\sum_\omega \ldots + \frac{1}{2}\sum_{-\omega} \ldots$, which gives

$$(-1)^{N+F} \frac{T^{N+1}}{2V^{N+1}} \sum_{I=0,1} \sum_{\omega,\mathbf{p}} \frac{1}{[(-1)^I i\omega_1 - \xi_{\mathbf{p}_1}]^2} \frac{1}{(-1)^I i\omega_2 - \xi_{\mathbf{p}_2}} \ldots \frac{1}{(-1)^I i\omega_{2N} - \xi_{\mathbf{p}_{2N}}} D(\Omega_1, \mathbf{p}_1) \ldots D(\Omega_N, \mathbf{p}_N). \tag{2.23}$$

The value of the topologically equivalent diagram contributing to ρ_s in the dual disordered non-interacting system is given by

$$\frac{(-1)^{N+F}}{V^{N+1}\ell_{d+1}^{N+1}} \sum_{\mathbf{p},k} \mathrm{Tr} \left[\hat{\sigma}_z \frac{1}{-k_1\hat{\sigma}_y - \xi_{\mathbf{p}_1}\hat{\sigma}_z} \frac{\hat{\sigma}_z}{2} \frac{1}{-k_1\hat{\sigma}_y - \xi_{\mathbf{p}_1}\hat{\sigma}_z} \hat{\sigma}_z \ldots \hat{\sigma}_z \frac{1}{-k_{2N}\hat{\sigma}_y - \xi_{\mathbf{p}_{2N}}\hat{\sigma}_z} \right] \widetilde{D}(K_1, \mathbf{p}_1) \ldots \widetilde{D}(K_N, \mathbf{p}_N), \tag{2.24}$$

where $(k_i, \mathbf{p}_i)$ is a $d+1$-dimensional momentum; $i = 0, 1, \ldots 2N-1$; $\mathrm{Tr}\ldots$ is taken with respect to the pseudospin degrees of freedom; (anti-)periodic boundary conditions have to be chosen along the $d+1$-st dimension for mapping to the (fermionic) bosonic particles in the interacting system; $-\widetilde{D}(K_i, \mathbf{p}_i)$ is the Fourier-transform of the impurity lines. Similar to the interacting diagrams, the summation is carried over $N+1$ independent momenta, with the other momenta determined by the momentum conservation laws. In

Eq. 2.24, the particle propagator is defined as

$$(-k_i\hat{\sigma}_y - \xi_{\mathbf{p}_i}\hat{\sigma}_z)^{-1} = \frac{1}{2}\left[G^A(k_i,\mathbf{p}_i,E=0) + G^R(k_i,\mathbf{p}_i,E=0)\right], \tag{2.25}$$

where G^A and G^R are the advanced and retarded Green's functions of a free particle.

Equation (2.24) can be rewritten as

$$\frac{(-1)^{N+F}}{2V^{N+1}\ell_{d+1}^{N+1}}\sum_{\mathbf{p},k}\mathrm{Tr}\left[\frac{1}{ik_1\hat{\sigma}_x - \xi_{\mathbf{p}_1}\mathbb{1}_{2\times2}}\frac{1}{ik_1\hat{\sigma}_x - \xi_{\mathbf{p}_1}\mathbb{1}_{2\times2}}\cdots \right.$$
$$\left.\frac{1}{ik_{2N}\hat{\sigma}_x - \xi_{\mathbf{p}_{2N}}\mathbb{1}_{2\times2}}\right]\widetilde{D}(K_1,\mathbf{p}_1)\ldots\widetilde{D}(K_N,\mathbf{p}_N), \tag{2.26}$$

where $\mathbb{1}_{2\times2}$ is the identity matrix in the pseudospin space.

Since all the propagators in the square bracket commute with each other, we can again replace the operator $\hat{\sigma}_x$ with its eigenvalues $(-1)^I$ with $I = 0, 1$. Then, Eq. (2.26) can be rewritten as

$$\frac{(-1)^{N+F}}{2V^{N+1}\ell_{d+1}^{N+1}}\sum_{I=0,1}\sum_{\mathbf{p},k}\left[\frac{1}{i(-1)^Ik_1 - \xi_{\mathbf{p}_1}}\frac{1}{i(-1)^Ik_1 - \xi_{\mathbf{p}_1}}\cdots \right.$$
$$\left.\frac{1}{i(-1)^Ik_{2N} - \xi_{\mathbf{p}_{2N}}}\right]\widetilde{D}(K_1,\mathbf{p}_1)\ldots\widetilde{D}(K_N,\mathbf{p}_N). \tag{2.27}$$

This matches the value of the corresponding diagram for the interacting system Eq. (2.23), so long as $\ell_{d+1} = 1/T$ and the Matsubara frequencies ω_i in Eq. (2.23) match the values of the momenta k_i in Eq. (2.27).

In summary, we have established the correspondence, to all orders of the perturbation theory, between observables in a d-dimensional bosonic (fermionic) interacting disorder-free system at temperature T and a dual $d+1$-dimensional non-interacting disordered system of length $\ell_{d+1} = 1/T$ with (anti-)periodic boundary conditions along

the $d+1$-st dimension. For the corresponding observables, when the screening effects can be neglected in the interacting system, all diagrams at each order in perturbation theory can be one-to-one mapped to topologically equivalent diagrams, whose values have been shown to be equal.

In the next subsection, I will further demonstrate the derivation of the duality by considering explicitly several lowest-order diagrams contributing to $\langle \hat{n}(\mathbf{r}) \rangle$ and $\langle \hat{\rho}_s(\boldsymbol{\rho}) \rangle_{\rm dis}$.

2.3.2 Zeroth- and first-order diagrams

The concentration of particles at the zeroth order is given by

$$\langle \hat{n}^{(0)}(\mathbf{r}) \rangle = \frac{T}{V} \sum_{\omega,\mathbf{p}}{}' \frac{(-1)^F}{i\omega - \xi_{\mathbf{p}}} = \frac{1}{V} \sum_{\mathbf{p}} \frac{1}{\exp\left(\xi_{\mathbf{p}}/T\right) \mp 1}, \tag{2.28}$$

where $\sum'$ is the regularised sum over Matsubara frequencies. This corresponds to, e.g., an infinitesimal phase correction to the frequencies [42] $i\omega \to i\omega e^{-i\omega\delta}$, which ensures that the sum of Matsubara Green's function over frequencies gives the Bose (Fermi) distribution function for bosonic (fermionic) frequencies.

For the disordered system, the zeroth-order contribution to the dual observable is given by

$$\langle \rho_s^{(0)}(\boldsymbol{\rho}) \rangle_{\rm dis} = \frac{(-1)^F}{V \ell_{d+1}} \sum_{\mathbf{p},k}{}' \mathrm{Tr} \left[\frac{\hat{\sigma}_z}{2} \frac{1}{-k\hat{\sigma}_y - \xi_{\mathbf{p}} \hat{\sigma}_z} \right] = \frac{1}{V} \sum_{\mathbf{p}} \frac{1}{\exp\left(\xi_{\mathbf{p}} \ell_{d+1}\right) \pm 1}, \tag{2.29}$$

where "+" and "−" correspond to periodic and antiperiodic boundary conditions along the $d+1$-st dimension, respectively. Equations (2.28) and (2.29) are exactly equal for $\ell_{d+1} = 1/T$, in accordance with the duality transformation derived in this paper.

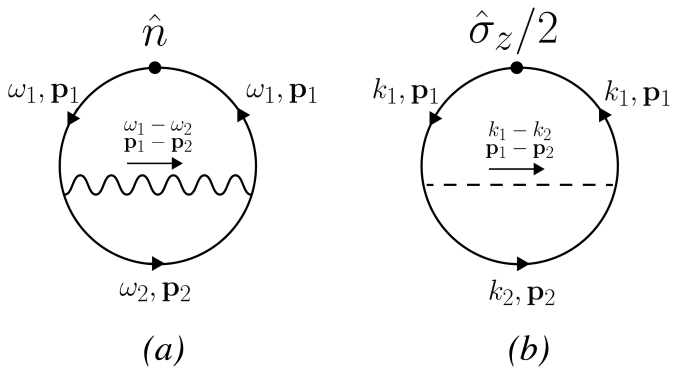

Figure 2.3: First-order diagrams for the density $\hat{n}$ in interacting disorder-free (a) and the operator ρ_s in non-interacting disordered (b) systems.

The first-order correction to $\langle \hat{n} \rangle$ is shown in Fig. 2.3a. The value of this diagram is given by

$$(-1)^{F+1} \frac{T^2}{V^2} \sum_{\omega_1, \omega_2, \mathbf{p}_1, \mathbf{p}_2} \frac{1}{(i\omega_1 - \xi_{\mathbf{p}_1})^2} \frac{1}{i\omega_2 - \xi_{\mathbf{p}_2}} D(\omega_1 - \omega_2, \mathbf{p}_1 - \mathbf{p}_2). \tag{2.30}$$

Again, since the bosonic propagator is even under the inversion of Matsubara frequency, $D(\omega_1 - \omega_2, \mathbf{p}_1 - \mathbf{p}_2) = D(-\omega_1 + \omega_2, \mathbf{p}_1 - \mathbf{p}_2)$, the sum with respect to the frequencies in Eq. (2.30) can be equivalent written as two sums: $\sum_{\omega_1, \omega_2} \ldots = \frac{1}{2} \sum_{\omega_1, \omega_2} \ldots + \frac{1}{2} \sum_{-\omega_1, -\omega_2} \ldots$. Therefore, Eq.(2.30) can be rewritten as

$$(-1)^{F+1} \frac{T^2}{2V^2} \sum_{\omega_1, \omega_2, \mathbf{p}_1, \mathbf{p}_2} \left[\frac{1}{(i\omega_1 - \xi_{\mathbf{p}_1})^2} \frac{1}{i\omega_2 - \xi_{\mathbf{p}_2}} + \frac{1}{(-i\omega_1 - \xi_{\mathbf{p}_1})^2} \frac{1}{-i\omega_2 - \xi_{\mathbf{p}_2}} \right]$$
$$\times D(\omega_1 - \omega_2, \mathbf{p}_1 - \mathbf{p}_2). \tag{2.31}$$

The corresponding diagram for the non-interacting disordered system con-

tributing to ρ_s is shown in Fig. 2.3b and the value is given by

$$\frac{(-1)^F}{V^2\ell_{d+1}^2}\sum_{\mathbf{p}_1,\mathbf{p}_2,k_1,k_2}\mathrm{Tr}\left[\hat{\sigma}_z\frac{1}{-k_1\hat{\sigma}_y-\xi_{\mathbf{p}_1}\hat{\sigma}_z}\frac{\hat{\sigma}_z}{2}\frac{1}{-k_1\hat{\sigma}_y-\xi_{\mathbf{p}_1}\hat{\sigma}_z}\hat{\sigma}_z\frac{1}{-k_2\hat{\sigma}_y-\xi_{\mathbf{p}_2}\hat{\sigma}_z}\right]$$
$$\times\left[-\widetilde{D}(k_1-k_2,\mathbf{p}_1-\mathbf{p}_2)\right] \tag{2.32}$$

Multiplying $\hat{\sigma}_z$ on both numerators and denominators and taking the trace with respect to the eigenvalues of $\hat{\sigma}_x$ gives

$$\frac{(-1)^{F+1}}{2V^2\ell_{d+1}^2}\sum_{\mathbf{p}_1,\mathbf{p}_2,k_1,k_2}\left(\frac{1}{ik_1-\xi_{\mathbf{p}_1}}\frac{1}{ik_1-\xi_{\mathbf{p}_1}}\frac{1}{ik_2-\xi_{\mathbf{p}_2}}\right.$$
$$\left.+\frac{1}{-ik_1-\xi_{\mathbf{p}_1}}\frac{1}{-ik_1-\xi_{\mathbf{p}_1}}\frac{1}{-ik_2-\xi_{\mathbf{p}_2}}\right)\widetilde{D}(k_1-k_2,\mathbf{p}_1-\mathbf{p}_2). \tag{2.33}$$

The values Eqs. (2.31) and (2.33) are equal, since the values of ω_i and k_i match. This directly follows from the choice of the boundary conditions and $\ell_{d+1}=1/T$, specified in the summary of the mapping, Table. 2.1.

2.4 Example – quantum dot and disordered wire

In this section, I provide an example of equivalent systems by the duality mapping. The interacting system is a one-site Hubbard model (quantum dot) described by the Hamiltonian

$$\hat{\mathcal{H}}_{dot}=\xi\hat{n}_\uparrow+\xi\hat{n}_\downarrow-g\hat{n}_\uparrow\hat{n}_\downarrow, \tag{2.34}$$

where ξ is a constant describing the energy between the two levels of the quantum dot (see Fig. 2.4), and $n_\uparrow$ and $n_\downarrow$ are the numbers of the electrons in the "spin up" and "spin down" states.

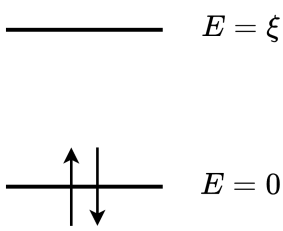

Figure 2.4: Energy levels of the one-site Hubbard model.

The quantum dot is mapped to a one-dimensional disordered wire model, described by the Hamiltonian

$$\hat{h}_{wire} = \sum_{i=\uparrow,\downarrow} \hat{\Psi}_i(x) \left[\xi\hat{\sigma}_z - i\hat{\sigma}_y\partial_x + u(x)\hat{\sigma}_z\right] \hat{\Psi}_i(x). \tag{2.35}$$

Here, $u(x)$ is the one-dimensional random potential, which is short-range correlated with the disorder strength given by

$$\int \langle u(x)u(x')\rangle dx' = g. \tag{2.36}$$

To see Eq. (2.34) maps to Eq. (2.35) by the duality, we can first rewrite the Hamiltonian Eq. 2.34 in an equivalent form

$$\hat{\mathcal{H}}_{dot} = \left(\xi + \frac{g}{2}\right) \hat{n}_\uparrow + \left(\xi + \frac{g}{2}\right) \hat{n}_\downarrow - \frac{g}{2} \left(\hat{n}_\uparrow + \hat{n}_\downarrow\right)^2, \tag{2.37}$$

where we have used that $\hat{n}^2_{\uparrow,\downarrow} = \hat{n}_{\uparrow,\downarrow}$. The partition function of this quantum dot system is given by

$$Z = \int \mathcal{D}\bar{\Psi}\mathcal{D}\Psi\, e^{-\int_0^\beta \sum_{i=\uparrow,\downarrow} \bar{\Psi}_i(\tau)\left[\partial_\tau + \xi + \frac{g}{2}\right]\Psi_i(\tau)\, d\tau - \frac{g}{2}\int_0^\beta \left[\sum_{i=\uparrow,\downarrow} \bar{\Psi}_i(\tau)\Psi_i(\tau)\right]^2 d\tau}. \tag{2.38}$$

Decoupling the quartic term by an HS field ϕ gives

$$Z = \int \mathcal{D}\bar{\Psi}\mathcal{D}\Psi\mathcal{D}\phi\, e^{-\int_0^\beta \sum_{i=\uparrow,\downarrow} \bar{\Psi}_i(\tau)\left[\partial_\tau + \xi + \frac{g}{2} + \phi(\tau)\right]\Psi_i(\tau)\, d\tau - \frac{1}{2g}\int_0^\beta \phi^2(\tau)\, d\tau}. \tag{2.39}$$

Applying the established duality transformation, this model can be mapped to the disordered non-interacting model given in Eq. (2.35), with the bosonic field $\phi(\tau)$ mapped to a random potential $u(x)$ and the Matsubara time τ mapped to the coordinate x. The dual disorder potential is short-ranged with the strength described by the coupling constant g.

Strictly speaking, the one-site Hubbard model Eq. (2.34) does not satisfy the assumption of the mapping since the screening effects and the Hartree-type contributions are not negligible. For example, diagram (a) in Fig. 2.5 corresponds to the Hartree contribution to the average occupation number $\langle \hat{n}_\sigma \rangle$ with spin σ, whose value is equal to diagram (b), and therefore, is not negligible. However, observables that are unaffected by the screening diagrams in the quantum dot model can still be mapped to the observables in the disordered wire system. As an example, the following number correlator

$$K = \langle \hat{n}_\uparrow \hat{n}_\downarrow \rangle - \langle \hat{n}_\uparrow \rangle \langle \hat{n}_\downarrow \rangle \tag{2.40}$$

is not affected by the screening or Hartree contributions to the first order in g. The diagrams that contribute to the correlator K are shown in Fig. 2.5, which do not involve screening and Hartree effect, to the leading order in coupling g. The value of the correlator is given by

$$K = [2.5c] + o(g^2) = \frac{g}{T} \left[\frac{e^{\xi/T}}{(1+e^{\xi/T})^2} \right]^2 + o(g^2). \tag{2.41}$$

The correlator can also be computed directly in the equilibrium state at temperature

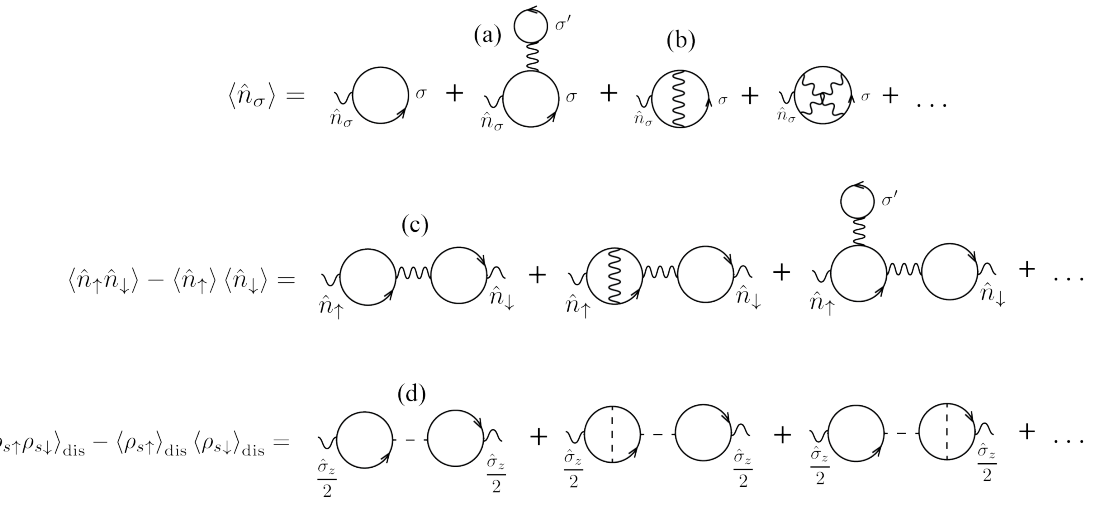

Figure 2.5: Diagrams that contribute to the correlators K of the one-site Hubbard model Eq. (2.34) and $K_{\rm dis}$ of the disordered wire Eq. (2.35). K and $K_{\rm dis}$ are defined in Eqs. (2.40) and (2.44), respectively

T, and is given by

$$K = \frac{\sum_{n_\uparrow,\downarrow=0,1} n_\uparrow n_\downarrow e^{-\frac{n_\uparrow\xi+n_\downarrow\xi-gn_\uparrow n_\downarrow}{T}}}{\sum_{n_\uparrow,\downarrow=0,1} e^{-\frac{n_\uparrow\xi+n_\downarrow\xi-gn_\uparrow n_\downarrow}{T}}} - \left(\frac{\sum_{n_\uparrow,\downarrow=0,1} n_\uparrow e^{-\frac{n_\uparrow\xi+n_\downarrow\xi-gn_\uparrow n_\downarrow}{T}}}{\sum_{n_\uparrow,\downarrow=0,1} e^{-\frac{n_\uparrow\xi+n_\downarrow\xi-gn_\uparrow n_\downarrow}{T}}}\right)^2 \tag{2.42}$$

$$= \frac{g}{T}\left[\frac{e^{\xi/T}}{(1+e^{\xi/T})^2}\right]^2 + o(g^2), \tag{2.43}$$

where we again kept only the leading contribution in g in the last equality.

Since the leading order contributions to the correlator K do not involve screening or Hartree contributions, it can be mapped to an observable in the dual disordered wire system.

$$K_{\rm dis} = \langle\rho_{s\uparrow}\rho_{s\downarrow}\rangle_{\rm dis} - \langle\rho_{s\uparrow}\rangle_{\rm dis}\langle\rho_{s\downarrow}\rangle_{\rm dis}. \tag{2.44}$$

The diagrams contributing to the correlator $K_{\rm dis}$ are shown in Fig. 2.5. The leading

order contribution to $K_{\rm dis}$ is given by

$$\begin{aligned} K_{\rm dis} &= [2.5d] + o(g^2) \\ &= \frac{g}{\ell_{d+1}^3} \left[\sum_{k_1} \mathrm{Tr} \left(\hat{\sigma}_z \frac{1}{-k_1 \hat{\sigma}_y - \xi \hat{\sigma}_z} \frac{\hat{\sigma}_z}{2} \frac{1}{-k_1 \hat{\sigma}_y - \xi \hat{\sigma}_z} \right) \right]^2 + o(g^2) \\ &= \frac{g}{\ell_{d+1}^3} \left(\sum_{k_1} \frac{-k_1^2 + \xi^2}{\left(k_1^2 + \xi^2\right)^2} \right)^2 = g\, \ell_{d+1} \left[\frac{e^{\xi \ell_{d+1}}}{(1 + e^{\xi \ell_{d+1}})^2} \right]^2 + o(g^2). \end{aligned} \tag{2.45}$$

Because the quantum dot described by the Hamiltonian (2.34) is fermionic, the dual disordered wire described by the Hamiltonian (2.35) has antiperiodic boundary conditions. Since $\ell_{d+1} = 1/T$, Eqs. (2.41) and (2.45) are exactly equal, as expected from the duality mapping.

2.5 Types of dual systems and outlook

The Hamiltonian Eq. (2.1) and (2.2) describe multiple types of interacting and disordered systems. As shown in Table. 2.2, these systems can be broadly classified into three classes. The mapping is exact for the first case — $\xi_{\mathbf{p}}$ vanishes at a point. The screening effect is, in general, non-negligible for the case with $\xi_{\mathbf{p}}$ vanishes at a surface since the DoS is non-zero at the fermi level. However, for physical properties where screening effects are unimportant, the mapping can still be carried out. As an example, systems with a finite Fermi surface can undergo a BCS transition. Near the phase transition, the dominant diagrams are ladder diagrams, which do not involve particle loops, and therefore, can be mapped to a disorder-driven instability for the dual disordered system. I will discuss this in more detail in Sec. 3.2. The mapping for

	Interacting model	Disordered model
$\xi_{\mathbf{p}}$ vanishes at a point ($\mathbf{p} = 0$)	Nodal-point semimetal or dilute gas with power-law dispersion	Anisotropic nodal-point semimetal
$\xi_{\mathbf{p}}$ vanishes at a surface	Metal	Nodal-line semimetal
p_{d+1} constrained	Systems at very high temperatures	Nodal-point semimetal (isotropic)

Table 2.2: Three classes of equivalent interacting and disordered systems.

the third case is not exact.

The duality mapping is powerful because it allows for predictions of new phase transitions by mapping previously known ones. In the following two chapters, I will show one example of new phase transitions for each of the three types of systems.

For the first case, the duality maps the BEC-vacuum transition for dilute gas of bosons at zero temperature to a disorder-driven transition for disordered nodal-point semimetals (Sec. 3.1). For the second case, the BCS transition of a 2-dimensional metal is mapped to a disorder-driven transition of a 3-dimensional nodal-line semimetal. Though for the third case, the case with p_{d+1} constrained, the mapping is not exact, it still allows us to predict a high-temperature interaction-driven transition in a system with power-law dispersions $\xi_{\mathbf{p}} \propto p^{\alpha}$, through a mapping of the non-Anderson disorder-driven transitions [19] for particles with the same dispersion in the same dimension. I

will discuss this transition in more detail in Chap. 4.

Chapter 3

Unconventional phase transitions in disordered semimetals

The equivalence between interacting disorder-free systems and disordered non-interacting systems established in the previous section allows one to map interaction-driven phase transitions to disorder-driven phase transitions and vice versa. This is counterintuitive since it is a common belief that Anderson metal-insulator transition is the only type of disorder-driven transition in non-interacting disordered systems, and interacting disorder-free systems, on the other hand, undergo many types of interaction-driven transitions. However, Sec. 1.3 has shown disordered non-interacting systems with power-law dispersion in high dimensions can undergo disorder-driven transitions that are distinct from the Anderson transition. This suggests that there may exist more types of disorder-driven transition. Therefore, the duality mapping we established can be used as an effective tool to explore new disorder-driven transitions by mapping known

interaction-driven transitions to them. This chapter presents two examples of unconventional disorder-driven transitions that are predicted by mapping interaction-driven transitions. The first example is a disorder-driven transition in anisotropic nodal-point semimetals that is dual to the BEC-vacuum transition for power-law dispersing Bose gases with attractive interactions (Sec. 3.1); and the second example is a disorder driven transition in 3-dimensional nodal-line semimetals dual to the BCS superconducting transitions in 2-dimensional metals (Sec. 3.2).

3.1 Disorder-driven transition in a nodal-point semimetal

Dilute Bose gases with power-law dispersions $\xi_{\mathbf{k}} \propto |\mathbf{k}|^{\alpha}$ and short-range attractive interactions exhibit the so-called vacuum-BEC transition [43, 44, 45, 46] in low temperatures. The transition can be derived from an RG analysis of the coupling constant g describing the interaction strength, at chemical potential $\mu \to 0^{-}$, which yields an exact RG equation at zero temperature

$$\partial_l \gamma = (\alpha - d)\gamma + \gamma^2 \tag{3.1}$$

under the rescaling of the length scale by a factor of e^{ℓ}. Here, γ is the dimensionless coupling constant defined as

$$\gamma = \frac{S_d}{2(2\pi)^d} g K^{d-\alpha}, \tag{3.2}$$

where S_d is the volume of a unit d-dimensional sphere, and K is the ultraviolet momentum cutoff. The RG equation Eq. (3.1) describes the RG flow as shown in Fig. 3.1. In low dimensions, $d < \alpha$, the effects of attractive interactions grow at long-wavelength

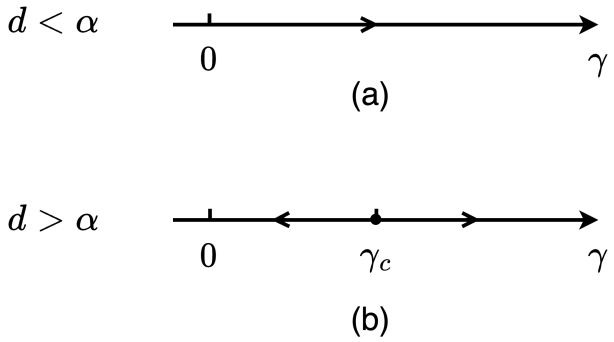

Figure 3.1: The RG flow of Eq. (3.1). γ is the dimensionless coupling constant. In the interacting Bose gas system, γ describes the interaction strength. In the dual disordered system, γ describes the disorder strength. In high dimensions, $d > \alpha$, the unstable fixed point at $\gamma = \gamma_c$ describes a phase transition. In the interacting system, this phase transition is the BEC-vacuum transition between a weakly interacting (vacuum) phase and a strongly interacting (BEC) phase. In the disordered system, the phase transition is between an effective disorder-free phase and a strongly disordered phase.

and the system is unstable. In high dimensions, $d > \alpha$, the RG flow has an infrared unstable fixed point at $\gamma_c = d - \alpha$. Interactions weaker than the critical interaction strength $\gamma < \gamma_c$ renormailzes to zero at long wavelength; and interactions stronger than the critical value $\gamma > \gamma_c$ grows under renormalization. Therefore, the RG fixed point at γ_c distinguishes a phase with effectively non-interacting particles (the vacuum phase) and a phase of strongly correlated particles (the BEC phase). The particle number is zero at chemical potential $\mu \to 0^-$ for the effectively non-interacting phase and non-zero for the strongly correlated phase, and can be used as an order parameter to distinguish the two phases.

The dual disordered system is $d+1$-dimensional and is described by the Hamiltonian

$$\hat{h} = \hat{\sigma}_z \xi_{\hat{\mathbf{p}}} + \hat{\sigma}_y p_{d+1} + \hat{\sigma}_z u(\boldsymbol{\rho}), \tag{3.3}$$

where $\xi_{\mathbf{k}}$ is chosen to be the same form as the dispersion of the interacting system, and the disorder potential is short-range correlated with the disorder strength described by the same coupling constant g. The RG equation Eq. (3.1) can be mapped exactly to the disordered system, where now the unstable fixed point in dimensions $d > \alpha$ describes a disorder-driven phase transition between an effectively disorder-free phase and a strongly disordered phase. This disorder-driven transition manifests itself in the critical behaviour of observables, such as the DoS and transport coefficients in the system. In contrast to the non-Anderson disorder-driven transitions [19] introduced in Sec. 1.3, the transition predicted here is described exactly by the RG equation (3.1), which allows for an exact determination of the correlation-length critical exponent $\nu = 1/(d-\alpha)$.

3.1.1 Details of the RG analysis for interacting Bose gases and disordered semimetals

This section provides the details of the RG analysis. As we will show, the renormalization of the interaction strength for the interacting Bose gas and the disorder strength for the dual disordered nodal-point semimetal is described by the same RG flow equation (3.1), which follows directly from the duality transformation between the two systems.

The RG procedure for the interacting system involves repeatedly integrating out shells of largest momenta,

$$Ke^{-l} \leq |\mathbf{k}| \leq K. \tag{3.4}$$

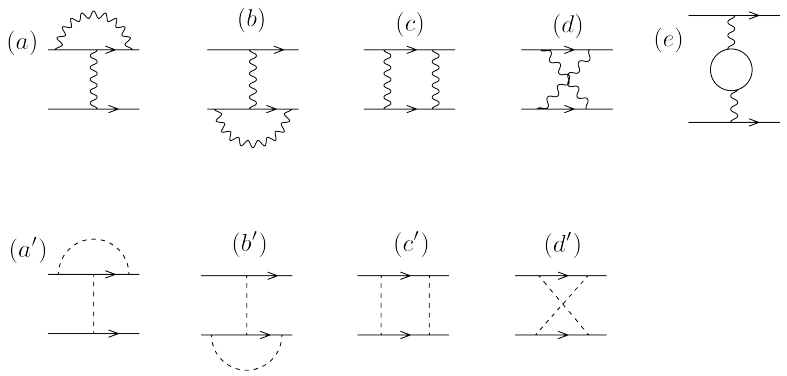

Figure 3.2: Diagrams for the renormalization of the coupling constants in the interacting Bose gas [(a)–(e)] and the disordered nodal-point semimetal [(a′)–(d′)].

This procedure renormalizes the parameters in the original theory, for example, the interaction strength g and the chemical potential μ. The diagrams for the one-loop renormalization of the interaction strength are shown in Figs. 3.2(a)–3.2(e). When evaluating these diagrams, it is sufficient to set all external incoming and outgoing frequencies and momenta to zero and sum/integrate only with respect to intermediate frequencies and momenta. At low temperatures, the dominant contribution comes from diagram Fig. 3.2(c), and is given by

$$[3.2c] = g^2 \int_\omega \int_{\mathbf{k}} \frac{1}{i\omega - \hat{\xi}_{\mathbf{k}}} \otimes \frac{1}{-i\omega - \hat{\xi}_{-\mathbf{k}}} \tag{3.5}$$

Here, we approximated the Matsubara frequency summation as an integral $T\sum_{i\omega} \ldots \to \int \frac{d\omega}{2\pi} \ldots$ for low temperatures; the integration with respect to the momentum $\mathbf{k}$ are carried out over the momentum shell (3.4); the dispersion $\xi_{\mathbf{k}} \propto k^\alpha$ has the power dependence on the momentum $\mathbf{k}$, but may also have additional structure in the valley or spin space; $\otimes$ is the product of the spin/valley subspaces corresponding to the top and bottom propagators in Fig. 3.2(c). For a scalar dispersion, $\xi_{\mathbf{k}} = |\mathbf{k}|^\alpha$, which has no

valley and spin structure, the renormalized interaction strength has a trivial structure in the spin/valley space, and is given by

$$\delta g = [3.2c] = \frac{g^2 S_d K^{d-\alpha}}{2(2\pi)^d} \frac{1 - e^{-(d-\alpha)l}}{d-\alpha}. \tag{3.6}$$

This leads to the RG flow equation for the interaction strength

$$\partial_l g = \frac{S_d K^{d-\alpha}}{2(2\pi)^d} g^2. \tag{3.7}$$

Introducing the dimensionless coupling constant

$$\gamma = \frac{S_d}{2(2\pi)^d} g K^{d-\alpha}, \tag{3.8}$$

we can write the one-loop RG flow equation as

$$\partial_l \gamma = (\alpha - d)\gamma + \gamma^2. \tag{3.9}$$

It has been shown in Ref. [43] that the RG flow equation (3.9) is exact, i.e. applies beyond the one-loop approximation. The renormalization of the interaction strength is given by the set of ladder diagrams shown in Fig. (3.3), and therefore can be described by an iterative equation. This leads directly to an exact form of the RG equation (3.9).

The diagrams contributing to the renormalization of the disorder strength of the dual disordered non-interacting system, described by the Hamiltonian (3.3), are shown in Figs. 3.2(a′)–3.2(d′). Each of these four diagrams can be mapped to the diagrams 3.2(a)–3.2(d) for the interacting Bose gas by the duality mapping. The diagrams in the disordered system do not include diagrams with a closed loop of particles, for

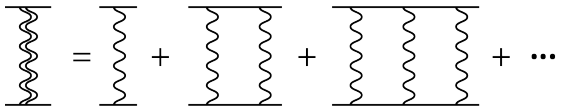

Figure 3.3: Ladder diagrams for the renormalization of the interaction strength.

example, Fig. 3.2(e). However, the contribution of such diagrams is suppressed for the interacting dilute Bose gas due to the low DoS at the chemical potential. Therefore, the renormalization of the interaction strength of the Bose gas can be mapped to the renormalization of the disorder strength of the dual disordered system order by order in perturbation theory.

The main contribution to the renormalization of the disorder strength g comes from Fig. 3.2(c′). While the other contributions to the renormalization are suppressed, it is convenient to evaluate Figs. 3.2(c′) and 3.2(d′) together:

$$
\begin{aligned}
&[3.2c'] + [3.2d'] \\
&= g^2 \int_{\mathbf{p}} \int_{p_{d+1}} \hat{\sigma}_z \left(\frac{1}{\xi_{\mathbf{p}} \hat{\sigma}_z + p_{d+1} \hat{\sigma}_y} + \frac{1}{\xi_{-\mathbf{p}} \hat{\sigma}_z - p_{d+1} \hat{\sigma}_y} \right) \hat{\sigma}_z \otimes \hat{\sigma}_z \frac{1}{\xi_{\mathbf{p}} \hat{\sigma}_z + p_{d+1} \hat{\sigma}_y} \hat{\sigma}_z \\
&= g^2 \int_{\mathbf{p}} \int_{p_{d+1}} \frac{2\xi_{\mathbf{p}}^2}{\left[\xi_{\mathbf{p}}^2 + p_{d+1}^2\right]^2} \hat{\sigma}_z \otimes \hat{\sigma}_z \\
&\approx \frac{g^2 S_d K^{d-\alpha}}{2(2\pi)^d} \frac{1 - e^{-(d-\alpha)l}}{d - \alpha}.
\end{aligned}
\tag{3.10}
$$

Therefore, the flow of the disorder strength can be derived and is again given by Eq. (3.9). The identical RG flows for the coupling in the interacting Bose gas and the non-interacting disordered system follow directly from the duality transformation established in the previous chapter.

In high dimensions, $d > \alpha$, the RG equation (3.9) has an unstable fixed point

at $\gamma_c = d - \alpha$, which corresponds to a phase transition. Systems with disorder strength weaker than the critical value γ_c belong to the effective disorder-free phase, in which the disorder strength renormalizes to zero. Systems with disorder strength stronger than the critical value below to the strongly disordered phase, with disorder strength renormalizes to a finite value. This disorder-driven phase transition extends the previously studied non-Anderson disorder-driven transitions discussed in Sec. 1.3.

3.2 BCS-like disorder-driven transition in nodal-line semimetal

In this section, I will show that the BCS superconducting transition of a 2-dimensional metal can be mapped to a disorder-driven instability of a 3-dimensional nodal-line semimetal using the established interaction-disorder duality. This is based on Zhu and Syzranov's work, Ref. [47].

According to the duality, a 2-dimensional metal can be mapped to a 3D non-interacting disordered nodal-line semimetal described by Hamiltonian

$$\hat{h} = v\left(|\mathbf{p} - p_F|\right)\hat{\sigma}_z + vk\hat{\sigma}_y + u(\boldsymbol{\rho})\hat{\sigma}_z, \tag{3.11}$$

where $\xi_{\mathbf{p}} = v\left(|\mathbf{p} - p_F|\right)$ is the quasiparticle dispersion near the Fermi surface in the 2-dimensional metal; $\mathbf{p} = (p_x, p_y)$ is the 2-dimensional momentum vector in the xy plane, in which the nodal line lies; p_F is the Fermi momentum; k is the momentum component along the z axis; v is the quasiparticle velocity in the directions perpendicular to the nodal line. The disorder potential $u(\boldsymbol{\rho})$ is short-range correlated, with the disorder

strength identical to the strength of the short-range attractive interaction in the BCS model of the 2-dimensional metal.

In general, the mapping from interacting 2-dimensional metal to disordered non-interacting nodal-line semimetal does not satisfy the requirement of low DoS at the Fermi surface. However, near the transition, the dominant diagrams that contribute to the renormalization of the interaction strength are the ladder diagrams, as shown in Fig. 3.3, which do not consist of particle loops. Therefore, the ladder diagrams in the Cooper and exciton channels of the 2D metal can be mapped to the diagrams in the disordered nodal-line semimetal that renormalizes the disorder strength. The renormalized disorder strength is given by

$$g_c = \frac{g_0}{2} \frac{\frac{p_F g_0}{2\pi v^2} \log \frac{vK}{|E|}}{1 - \frac{p_F g_0}{2\pi v^2} \log \frac{vK}{|E|}} \left(\hat{\sigma}_x \otimes \hat{\sigma}_x - \hat{\sigma}_z \otimes \hat{\sigma}_z \right), \tag{3.12a}$$

$$g_e = \frac{g_0}{2} \frac{\frac{p_F g_0}{2\pi v^2} \log \frac{vK}{|E|}}{1 - \frac{p_F g_0}{2\pi v^2} \log \frac{vK}{|E|}} \left(\hat{\sigma}_x \otimes \hat{\sigma}_x + \hat{\sigma}_z \otimes \hat{\sigma}_z \right), \tag{3.12b}$$

where g_c and g_e corresponds to renormalizations due to the Cooper and exciton channels, respectively; g_0 is the bare disorder strength; E is the quasiparticle energy; and K is the ultraviolet cutoff. The singularities of (3.12a) and (3.12b) are mapped to the singularities of the renormalized couplings in the interacting metal near the Cooper and exciton-condensation instabilities.

The singularity of the renormalized coupling leads to singular behavior in observables. For example, the DoS diverges as

$$\rho(g, E) \propto |g_c(E) - g|^{-2} |E| \tag{3.13}$$

for g smaller than the critical value $g_c(E)$ and crosses over to a constant as g approaches

$g_c(E)$, where the critical disorder strength is given by $g_c(E) \approx 2\pi v^2/p_F \log\left(\frac{vK}{|E|}\right)$. Therefore, as $E \to 0$ (approaches the nodal-line), the DoS crossover from 0 to finite as the disorder strength increases and approaches to the critical value.

Chapter 4

Finite temperature criticality in systems with power-law interactions

In this chapter, I will discuss the critical behavior of a d-dimensional dilute gas of bosons with power-law dispersion $\xi_{\mathbf{k}} = a|\mathbf{k}|^{\alpha}$, and short-range interactions characterized by a coupling constant g at a finite temperature T. In spatial dimensions $d > 2\alpha$, the system exhibits a phase transition between weakly and strongly interacting phases. This transition is similar to the non-Anderson disorder-driven phase transitions discussed in Sec. 1.3. The similarity is predicted by the established interaction-disorder duality presented in Chap. 2.

The phase transition can be realized in a trapped-ion spin system, the d-dimensional XXZ model with power-law interactions, described by the following Hamiltonian [48, 49, 50, 51]

$$\hat{H} = -\frac{1}{4}\sum_{i\neq j}\frac{J}{|i-j|^{d+\alpha}}\left(\hat{\sigma}_i^x\hat{\sigma}_j^x + \hat{\sigma}_i^y\hat{\sigma}_j^y + \Delta\hat{\sigma}_i^z\hat{\sigma}_j^z\right) - \frac{h}{2}\sum_i \hat{\sigma}_i^z\,. \tag{4.1}$$

Here, the external field polarizes spins along the $+z$-direction. Elementary magnetic excitations in the system correspond to spin flips, hereinafter referred to as magnons, which propagate with dispersion $\xi_{\mathbf{k}} \propto |\mathbf{k}|^{\alpha}$. The magnons are attractively interacting due to the z-z coupling. Therefore, the phase transition that will be derived in this chapter manifest itself in this spin model as a function of the coupling Δ along the z-direction and the temperature. The weakly and strongly coupling phases corresponds to a phase with free magnons and a phase with strongly-coupled magnons, and can be distinguished experimentally by measuring the spin correlation function in x direction.

In what follows, I will start by describing qualitatively the critical behavior of power-law dispersing bosons (Sec. 4.1), and providing a detailed RG analysis of the model in Sec. 4.2. Then, in Sec. 4.3, I will show that the RG analysis can be applied to and the derived phase transition can be realized in the power-law interacting XXZ model. Finally, in Sec. 4.4, I will discuss the similarity of this interaction-driven phase transition and the previously studied non-Anderson disorder-driven phase transition [19].

4.1 Critical behaviors for power-law dispersing bosons at finite temperature

For power-law dispersing bosons with short-range attractive interactions, $g < 0$, in spatial dimensions $d > 2\alpha$, the system exhibits a phase transition between a weakly interacting phase and a strongly interacting phase. In the former, the bosons are effectively non-interacting; they behave like an ideal gas. In the latter, the low-

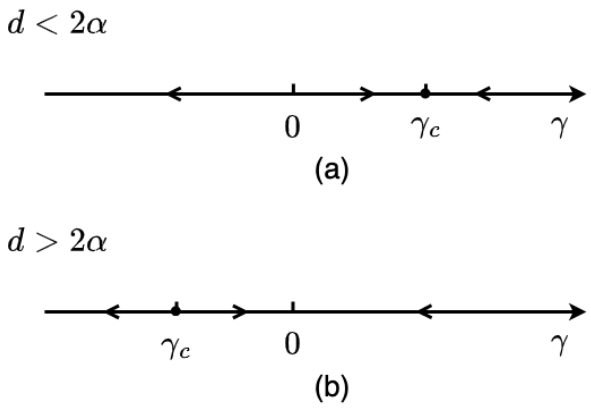

Figure 4.1: The renormalization group flow of Eq. (4.4), which describes the critical behavior of a dilute gas of power-law dispersing bosons $\xi_{\mathbf{k}} = a|\mathbf{k}|^{\alpha}$ with short-range interactions in spatial dimension d. Here, γ is the dimensionless coupling constant characterizing the interactions. $\gamma > 0$ corresponds to repulsive interactions. (a) In low dimensions, $d < 2\alpha$, there is a stable fixed point at $\gamma_c = 2\alpha - d > 0$, which describes the universal properties of the power-law dispersing bosons with repulsive interactions. (b) In high dimensions, $d > 2\alpha$, the fixed point at $\gamma_c = 2\alpha - d < 0$ is unstable and describes a phase transition for attractively interacting bosons.

energy quasiparticles are strongly interacting. As far as we know, such phase transition has not been previously studied in the literature and is the main focus of this paper. The phase transition can be derived via an RG analysis of the model. The RG flow is as shown in Fig. 4.1. In dimensions $d > 2\alpha$, the RG flow has an infrared unstable fixed point at $\gamma_c = -(d - 2\alpha)$, which corresponds to the phase transition describes above.

For bosons with short-range repulsive interactions, $g > 0$, in spatial dimensions $d < 2\alpha$, the system has a universal repulsive interaction strength. The universal repulsive interaction is described by the same RG fixed point, which is now infrared stable — the coupling constant renormalizes toward the fixed point at long wavelength. The spin model mentioned above can also serve as an example for this case. However, the study of universal properties of the spin model described by this fixed point will be

left for a future work.

4.2 Renormalization group analysis

In this section, I present a field-theoretical RG analysis of the model of power-law dispersing bosons with short-range interactions. The field theoretic action of such a boson, ψ, can be written as

$$S = \int d\tau d^d r \left[\psi^\dagger \left(\partial_\tau - \xi_{\hat{\mathbf{k}}} + \mu \right) \psi + \frac{g}{2} \psi^\dagger \psi^\dagger \psi \psi \right], \tag{4.2}$$

where the power-law dispersion $\xi_{\mathbf{k}} = a|\mathbf{k}|^\alpha$. Under renormalization, the coupling constant and the chemical potential are renormalized to values depends on the ultraviolet momentum cutoff K, $g(K)$ and $\lambda(K)$. In the subsection immediately follows, I will present the derivation of the set of RG equations that describe the flow of the parameters with respect to the ultraviolet cutoff scales. Before getting into the details of the derivations, I will first show the results.

Based on the derived RG flow equations, one can define a dimensionless coupling constant

$$\gamma = \frac{5 C_d}{a^2} g T K^{d-2\alpha}, \tag{4.3}$$

as a combination of the coupling constant g, the temperature T, and the ultraviolet momentum cutoff K. Here, $C_d = S_d/(2\pi)^d$ and S_d is the area of a unit sphere in d-dimensional spaces. Then, the RG equations for the dimensionless coupling constant γ and the parameter λ are given by

$$\partial_\ell \gamma = (2\alpha - d)\gamma - \gamma^2, \quad \partial_\ell \lambda = \frac{1}{5}\gamma\lambda. \tag{4.4}$$

The RG equation for γ determines the RG flow as shown in Fig. 4.1. $\gamma < 0$ corresponds to attractive interactions. In spatial dimensions $d > 2\alpha$, the RG equation has an unstable fixed point at $\gamma_c = -(d - 2\alpha)$, which suggests the power-law dispersing bosons with attractive interactions exhibit a phase transition at finite temperatures.

For attractive interactions, the system is unstable and energetically favorable to have a finite order parameter. Nevertheless, one can study the RG with a negative and small chemical potential $\mu \to 0^-$, where the system is stable when interactions are weak. In low dimensions, $d < 2\alpha$, the effects of attractive interactions grow at long-wavelength and the system becomes unstable. In high dimensions, $d > 2\alpha$, the RG equation has an unstable fixed point at $\gamma_c = 2\alpha - d < 0$. For $|\gamma| < |\gamma_c|$, the interaction strength renormalizes to zero at long wavelength, and the system is stable. For $|\gamma| > |\gamma_c|$, the effects of attractive interactions grow under renormalization and the system energetically favors a finite order parameter. Therefore, the RG fixed point for attractive interactions describes a phase transition between a phase with effectively non-interacting bosons and a phase of strongly coupled bosons.

The same RG equations also apply to short-range repulsive interactions, corresponding to the $\gamma > 0$ side of the diagram. In dimensions $d < 2\alpha$, the system has a stable RG fixed point at $\gamma_c = 2\alpha - d$, which suggests the power-law dispersing bosons at finite temperatures have a universal interaction strength for repulsive interactions.

4.2.1 Details of the RG analysis

The RG equations (4.4) are derived from a two-step RG analysis. We consider the system at a finite temperature T. In general, the system contains modes with higher energies compared to the scale set by the temperature, $\xi_{\mathbf{k}} > T$, and modes with lower energies, $\xi_{\mathbf{k}} < T$. However, near a critical point, the behavior of the system is dominated by the low-energy modes. Therefore, we perform the RG by the following two steps. First, we integrate out the higher energy modes from the ultraviolet cutoff to the scale $\xi_K \ll T$, which gives an effective theory of the low-energy modes. We then apply the RG analysis for the effective theory of the low-energy modes.

Initial renormalization

At one-loop order, integrating out the higher energy modes gives a correction to the self-energy of the following form

$$\Sigma^{(1)}(\omega, \mathbf{p}) = 2gT \sum_{\Omega}{}' \int_K^{K_\Lambda} \frac{d^d k}{(2\pi)^d} \frac{U(\mathbf{q}=0)}{i\Omega - \xi_{\mathbf{k}} + \mu} = 2g \int_K^{K_\Lambda} \frac{d^d k}{(2\pi)^d} n_B(\xi_{\mathbf{k}} - \mu) \approx 0. \quad (4.5)$$

Here, $\sum'$ is the regularised sum over Matsubara frequencies, (for example, infinitesimal phase corrections to the frequencies $i\omega \to i\omega e^{-i\omega\delta}$); K_Λ denotes the ultraviolet cutoff of the system; K is the ultraviolet cutoff of the low-energy effective theory; $n_B(\xi)$ is the Bose distribution function. The self-energy correction approximates to zero because the temperature is approximately zero compared to the energy of the modes being integrated out, which leads to $n_B(\xi_{\mathbf{q}} - \mu) \to 0$ for any $\xi_{\mathbf{q}} > 0$. Therefore, the initial renormalization does not correct the self-energy to all orders of perturbation theory.

The initial renormalization to the coupling constant g comes merely from the

ladder diagrams and is given by

$$\begin{aligned} g(K) &= g(K_\Lambda) - g(K_\Lambda)g(K)T\sum_\omega \int_K^{K_\Lambda} \frac{d^dq}{(2\pi)^d} \frac{1}{i\omega - \xi_{\mathbf{q}}} \frac{1}{-i\omega - \xi_{-\mathbf{q}}} \\ &= g(K_\Lambda) - g(K_\Lambda)g(K)\frac{S_d}{2(2\pi)^d}\frac{1}{a}\frac{1}{d-\alpha}\left(K_\Lambda^{d-\alpha} - K^{d-\alpha}\right). \end{aligned} \tag{4.6}$$

Therefore, the RG equations for λ and g are

$$\partial_\ell g = -\frac{C_d}{2a} g^2 K^{d-\alpha}, \quad \partial_\ell \lambda = 0. \tag{4.7}$$

Solving the equations determines the renormalized values

$$g(K) = \left[\frac{1}{g(K_\Lambda)} - \frac{1}{\tilde{g}_c} + \frac{1}{\tilde{g}_c}\left(\frac{K}{K_\Lambda}\right)^{d-\alpha}\right]^{-1}, \tag{4.8}$$

and $\lambda(K) = \lambda(K_\Lambda)$. Here, $C_d = S_d/(2\pi)^d$, with S_d being the area of a d-dimensional unit sphere, $\tilde{g}_c$ is the critical coupling constant, given by

$$\tilde{g}_c = -(d-\alpha)\frac{2a}{C_d} K_\Lambda^{d-\alpha}. \tag{4.9}$$

Therefore, in dimensions $d > \alpha$, for coupling constants much smaller than the critical value, $g(K_\Lambda) \ll \tilde{g}_c$, the contribution from the initial renormalization is higher order in $g(K_\Lambda)/g_c$ and is negligible, $g(K) \approx g(K_\Lambda)$.

For long-range interactions, $U(\mathbf{r}-\mathbf{r}') \propto -\frac{1}{|\mathbf{r}-\mathbf{r}'|^{d+\alpha}}$, with the power α the same as the power of the particle dispersion, a similar argument allows one to renormalize the long-range interaction to a short-range interaction, with the order of magnitude of the interaction strength remain unchanged.

"High temperature" RG

With the initial renormalization carried out, one can then perform an RG analysis to the low-energy effective theory whose ultraviolet energy cutoff scale is $\xi_K \ll T$. In other words, the low-energy theory is at a high temperature. The peculiarity of RG analyses at a high temperature comes from the Matsubara zero modes. The bosonic Matsubara frequencies are $\omega_n = 2n\pi T$ for $n \in Z$. At high temperatures, $T \gg \xi_K$, the absolute values of the frequencies $|\omega_n| \gg \xi_K$ for $n \neq 0$. Therefore, the zero frequency modes dominate the rest of the frequency modes in computing the renormalization of λ and g.

To be specific, let us consider the renormalization of the coupling constant g at high temperatures. The diagrams contributing to the renormalization of g to the one-loop order are shown in Fig. 4.2. Evaluating the diagrams at zero external frequency and momenta, we get

$$[4.2a] = [4.2b] = [4.2d] = [4.2e] = g^2 T \sum_\omega \int \frac{d^d k}{(2\pi)^d} \frac{1}{i\omega - \xi_{\mathbf{k}}} \frac{1}{i\omega - \xi_{\mathbf{k}}}$$
$$= g^2 T \sum_\omega \int \frac{d^d k}{(2\pi)^d} \frac{-\omega^2 + \xi_{\mathbf{k}}^2}{\left(\omega^2 + \xi_{\mathbf{k}}^2\right)^2}, \tag{4.10a}$$
$$[4.2c] = g^2 T \sum_\omega \int \frac{d^d k}{(2\pi)^d} \frac{1}{i\omega - \xi_{\mathbf{k}}} \frac{1}{-i\omega - \xi_{-\mathbf{k}}} = g^2 T \sum_\omega \int \frac{d^d k}{(2\pi)^d} \frac{1}{\omega^2 + \xi_{\mathbf{k}}^2}. \tag{4.10b}$$

Here, the momentum integration is carried out over a thin shell $Ke^{-\ell} < |\mathbf{k}| < K$, where K is the ultraviolet momentum cutoff. Since $\xi_K \ll T$, the zero Matsubara frequency modes dominate the rest of the frequency modes in the summations in (4.10). Therefore, the frequency summation can be replaced with only the zero mode contribution

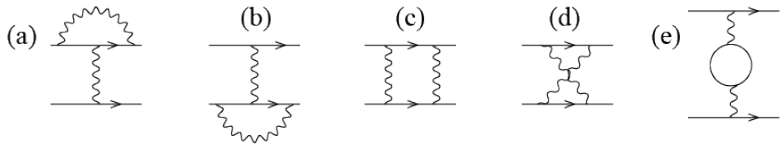

Figure 4.2: Diagrams renormalizing the coupling constants at one-loop order.

$T\sum_\omega \ldots \to T\delta(\omega)\ldots$, and Eqs. (4.10) can be rewritten as

$$[4.2a] = [4.2b] = [4.2c] = [4.2d] = [4.2e] = g^2 T \int_{Ke^{-\ell}<|\mathbf{k}|<K} \frac{d^d k}{(2\pi)^d} \frac{1}{\xi_{\mathbf{k}}^2}$$
$$= g^2 T C_d K^{d-2\alpha} \frac{1}{a^2} \frac{1-e^{-(d-2\alpha)\ell}}{(d-2\alpha)}. \qquad (4.11)$$

The RG flow equation for g with respect to ℓ can be derived and is given by

$$\partial_\ell g = -5g^2 T \frac{S_d K^{d-2\alpha}}{a^2(2\pi)^d} + o(g^2). \qquad (4.12)$$

Similarly, the renormalization for the chemical potential is also dominated by the contribution from the Matsubara zero modes. The renormalized Green's function is given by

$$G(i\omega, \mathbf{k}) = \frac{1}{i\omega - \xi_{\mathbf{k}} + \lambda\mu}, \qquad (4.13)$$

where λ is the parameter that describes the renormalization of the chemical potential. The correction to the chemical potential contains two contributions, one of which depends on μ and the other doesn't.

$$\lambda\mu \longrightarrow \lambda\mu + \lambda\cdot\delta\mu + \delta\lambda\cdot\mu \qquad (4.14)$$

Integration over a thin momentum shell $Ke^{-\ell} < |\mathbf{k}| < K$, gives the renormalization for

μ and λ. At one-loop order, we have

$$\delta\mu = -gT\sum_{\omega}\int_{Ke^{-\ell}<|\mathbf{k}|<K}\frac{d^dk}{(2\pi)^d}\frac{1}{i\omega-\xi_{\mathbf{k}}} \tag{4.15}$$

and

$$\delta\lambda = -\lambda gT\sum_{\omega}\int_{Ke^{-\ell}<|\mathbf{k}|<K}\frac{d^dk}{(2\pi)^d}\left(\frac{1}{i\omega-\xi_{\mathbf{k}}}\right)^2 \tag{4.16}$$

In these calculations, again, since $\xi_K \ll T$, zero frequency modes dominate the rest of the frequency modes. Therefore, we have

$$\delta\mu = gT\int_{Ke^{-\ell}<|\mathbf{k}|<K}\frac{d^dk}{(2\pi)^d}\frac{1}{\xi_{\mathbf{k}}} = gTS_dK^{d-\alpha}\frac{1}{a}\frac{1-e^{-(d-\alpha)\ell}}{(2\pi)^d(d-\alpha)} \tag{4.17}$$

and

$$\delta\lambda = \lambda gT\int_{Ke^{-\ell}<|\mathbf{k}|<K}\frac{d^dk}{(2\pi)^d}\frac{1}{\xi_{\mathbf{k}}^2} = \lambda gTS_dK^{d-2\alpha}\frac{1}{a^2}\frac{1-e^{-(d-2\alpha)\ell}}{(2\pi)^d(d-2\alpha)}. \tag{4.18}$$

This leads to the RG equation

$$\partial_\ell\lambda = \lambda\,\frac{gTS_d}{a^2(2\pi)^d}K^{d-2\alpha} \tag{4.19}$$

Based on the form of (4.12) and (4.19), one can define a dimensionless coupling constant Eq. 4.3, and rewrite the RG equations in simpler forms Eq. 4.4. Solving the RG equations with initial values $g(K_0) = g_0$ and $\lambda(K_0) = 1$, the renormalized $g(K)$ and $\lambda(K)$ can be derived

$$g(K) = \left[\frac{1}{g_0} - \frac{1}{g_c} + \frac{1}{g_c}\left(\frac{K}{K_0}\right)^{d-2\alpha}\right]^{-1}, \tag{4.20a}$$

$$\lambda(K) = \left(\frac{g(K)}{g_0}\right)^{\frac{1}{5}}, \tag{4.20b}$$

where K_0 is the UV cutoff, and $g_c = -(d-2\alpha)\,\frac{a^2}{5TC_d}K_0^{2\alpha-d}$ is the critical interaction strength.

The RG equations (4.4) allow to determine the correlation length critical exponent $\nu = 1/(d-2\alpha)$ and the dynamical critical exponent $z = \alpha + \frac{d-2\alpha}{5}$.

4.3 XXZ model with power-law interactions

Systems with bosonic power-law dispersing quasiparticles are ubiquitous. However, the phase transition we derived in the previous section exists when the spatial dimension of the system is higher than the lower critical dimension $d_c = 2\alpha$, where α is the power of the quasiparticle dispersion. Therefore, realistic systems exhibiting this transition are either in 3-dimension with linearly dispersing quasiparticles or lower dimensions with the power of quasiparticle dispersion $\alpha < 1$. This section focuses on the latter case. As we will show, the latter case and its phase transitions are accessible to trapped-ion experiments in 1 and 2 dimensions [48, 49, 50, 51]. We also present an experimental observable that exhibits singular behavior at the phase transition in the following section.

We study the d-dimensional XXZ model with power-law interactions and an external magnetic field applied in the z-direction, described by the Hamiltonian Eq. (4.1).

$$\hat{H} = -\frac{1}{4}\sum_{i\neq j}\frac{J}{|i-j|^{d+\alpha}}\left(\hat{\sigma}_i^x\hat{\sigma}_j^x + \hat{\sigma}_i^y\hat{\sigma}_j^y + \Delta\hat{\sigma}_i^z\hat{\sigma}_j^z\right) - \frac{h}{2}\sum_i \hat{\sigma}_i^z \tag{4.1}$$

Here, $\hat{\sigma}$s are the Pauli matrices; the interactions are ferromagnetic, $J, \Delta > 0$. We consider non-zero temperature, with $T < J$, and strong magnetic field $h \gg J$. By the following Holstein-Primakoff transformation, Eq. (4.1) can be exactly mapped to a Hamiltonian describing hard-core magnons with power-law dispersion and long-range

attractive interactions.

$$\hat{\sigma}_i^+ = 2\left(1-\hat{a}_i^\dagger\hat{a}_i\right)\hat{a}_i, \quad \hat{\sigma}_i^- = 2\hat{a}_i^\dagger\left(1-\hat{a}_i^\dagger\hat{a}_i\right), \quad \hat{\sigma}_i^z = 1-2\hat{a}_i^\dagger\hat{a}_i. \tag{4.21}$$

Here, $\hat{a}_i^\dagger$ and $\hat{a}_i$ are the creation and annihilation operators of the magnons (flipped spins). In momentum space, the Hamiltonian of the magnons can be written as

$$\hat{H} = \sum_{\mathbf{k}} \left(\xi_{\mathbf{k}} - \mu\right) \hat{a}_{\mathbf{k}}^\dagger \hat{a}_{\mathbf{k}} - \sum_{\mathbf{p}_1,\mathbf{p}_2,\mathbf{q}} U\left(\mathbf{q}\right) \hat{a}_{\mathbf{p}_1+\mathbf{q}}^\dagger \hat{a}_{\mathbf{p}_1} \hat{a}_{\mathbf{p}_2-\mathbf{q}}^\dagger \hat{a}_{\mathbf{p}_2}, \tag{4.22}$$

where

$$\xi_{\mathbf{k}} = c_2 J|\mathbf{k}|^\alpha, \quad \mu = -h + c_1 J(1-\Delta), \quad U(\mathbf{q}) = c_1 J\Delta - c_2 J\Delta|\mathbf{q}|^\alpha, \tag{4.23}$$

$U(\mathbf{q})$ is the long-range attractive interaction, with c_1 and c_2 being coefficients from the Fourier transformation of $1/|i-j|^{d+\alpha}$, defined as

$$c_1 = \frac{\pi^{\frac{d}{2}}\Gamma\left(\frac{\alpha}{2}\right)}{\Gamma\left(\frac{d+\alpha}{2}\right)}, \quad c_2 = -\frac{\pi^{\frac{d}{2}}\Gamma\left(-\frac{\alpha}{2}\right)}{\Gamma\left(\frac{d+\alpha}{2}\right)}. \tag{4.24}$$

Here, the lattice spacing is chosen to be unity. In Eq. (4.22), we omitted an on-site repulsive interaction term that prevents multiple bosons from occupying the same site. The on-site repulsion only renormalizes single-particle Green's functions and has no significance for our analysis below.

We see from Eq. (4.22) that the magnons have power-law dispersions $\xi_{\mathbf{k}} = c_2 J|\mathbf{k}|^\alpha$, and is a candidate of the phase transition derived in the previous section. Moreover, in trapped-ion experiments, the power α is continuously tunable, which allows one to bring the critical dimension arbitrarily close to the physical dimension of the system, ensuring the accuracy of our RG analysis. However, the chemical potential

for the magnons is a large negative number, in contrast to the close-to-zero chemical potential in our RG analysis. To get around this, one can impose a constraint on the magnetization to tune the chemical potential to the bottom of the magnon band. Experimentally, this corresponds to initializing the state with a few random spin flips, before letting it evolve with Hamiltonian (4.1). Since the Hamiltonian preserves magnetization in the z-direction, such experimental procedures are equivalent to imposing a constraint on the magnetization.

The interaction between magnons $U(\mathbf{q})$ has two terms: one depends on the momentum, and the other is independent of the momentum. For the long-wavelength magnons we focus on in this paper, its momentum is much smaller than the inverse lattice spacing $|\mathbf{q}| \ll 1$, and the term in $U(\mathbf{q})$ that depends on momentum is subdominant. Under the initial renormalization (see Sec. 4.2.1), the order of magnitude of the coefficients of both terms does not change, and the interaction can be approximated by a coupling constant

$$g = -2c_1 J\Delta. \tag{4.25}$$

We take this as the initial value of the coupling constant at the ultraviolet momentum cutoff K of the low-energy effective theory and take the initial value $\lambda(K) = 1$. Then, the dimensionless coupling at the cutoff K is equal to

$$\gamma(K) = -5C_d \frac{2c_1}{c_2^2} \frac{T\Delta}{J} K^{d-2\alpha}. \tag{4.26}$$

Besides K and dimensionless numbers, $\gamma(K) \propto T\Delta/J$. This allows us to derive a phase diagram as a function of the ratio T/J and Δ. In dimensions $d > 2\alpha$, the unstable

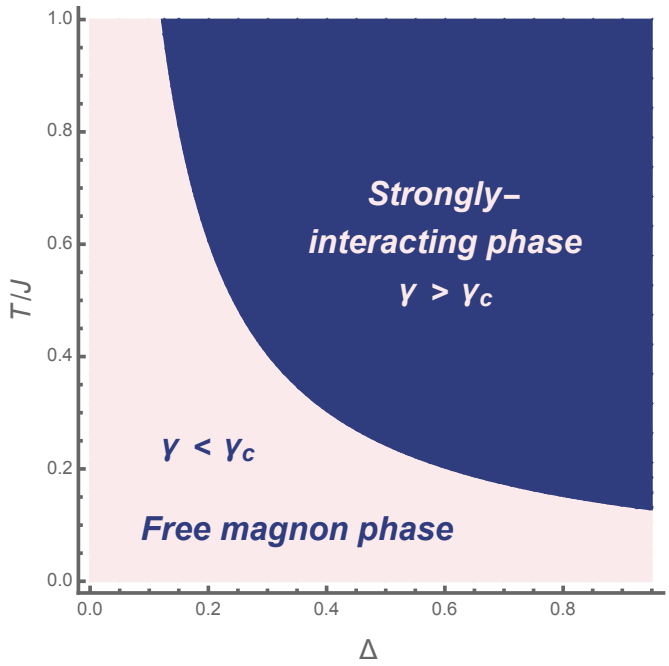

Figure 4.3: Phase diagram of the power-law dispersing magnons at finite temperature in $d = 1$, with $\alpha = 0.48$ for the dispersion. The phase boundary corresponds to the unstable RG fixed point at $\gamma_c = -0.04$. In the free magnon phase, the system behaves as a gas of effectively non-interacting magnons. While in the strongly interacting phase, the low-energy magnons are strongly coupled. Increasing temperature or the coupling in the z-direction can render a phase transition from the free magnon phase to the strongly interacting phase.

RG fixed point at $\gamma(K) = \gamma_c$ corresponds to a one-dimensional phase boundary in the Δ–T/J plane. The phase boundary separates a free magnon phase and a strongly interacting phase. For the region below the phase boundary, $|\gamma(K)| < |\gamma_c|$, the dimensionless coupling approaches 0 at long wavelength, and the low-energy magnons are effectively non-interacting. For the region above the phase boundary, $|\gamma(K)| > |\gamma_c|$, the dimensionless coupling grows at long wavelength, which corresponds to the phase of strongly coupled magnons. Fig. 4.3 shows the phase diagram for the 1-dimensional spin chain with $\alpha = 0.48$.

4.3.1 Experimental detection

The phase transition can be observed experimentally by measuring the spin correlation functions. Experimentally, one can first initialize the state with a few randomly flipped spins and then measure the spin correlation function in the x direction $\langle\sigma_i^x\sigma_j^x\rangle - \langle\sigma_i^x\rangle\langle\sigma_j^x\rangle$. This spin correlator is proportional to the renormalized single-particle Green's function

$$\langle\sigma_i^x\sigma_j^x\rangle - \langle\sigma_i^x\rangle\langle\sigma_j^x\rangle = \langle\hat{a}_i^\dagger\hat{a}_j\rangle + \langle\hat{a}_i\hat{a}_j^\dagger\rangle = -2G\left(\tau = 0, |\mathbf{r}_i - \mathbf{r}_j|\right). \tag{4.27}$$

The renormalized Green's function in the frequency and momentum space is

$$G(i\omega, \mathbf{k}) = \frac{1}{i\omega - \xi_{\mathbf{k}} - \Sigma(\omega, \mathbf{k})}, \tag{4.28}$$

where $\Sigma(\omega, \mathbf{k})$ is the self-energy, which, in the first Born approximation, is equal to

$$\Sigma(\omega, \mathbf{k}) = 2gT\sum_{\Omega}{}' \int_0^K \frac{d^dq}{(2\pi)^d}\frac{1}{i\Omega - \xi_{\mathbf{q}}} \approx -2gT\int_0^K \frac{d^dq}{(2\pi)^d}\frac{1}{\xi_{\mathbf{q}}}, \tag{4.29}$$

where $\sum'$ is the regularised sum over Matsubara frequencies, g is the renormalized coupling constant, and the integral in the last equality is equal to the number of low-energy magnons. In the free magnon phase, the self-energy correction is small due to the low number of magnon excitations, and the spin correlation is approximately equal to

$$\langle\sigma_i^x\sigma_j^x\rangle \approx T\int \frac{d^dk}{(2\pi)^d}\frac{e^{ik|\mathbf{r}_i - \mathbf{r}_j|}}{\xi_{\mathbf{k}}} = \frac{T}{c_2 J}C_d\int \frac{e^{ik|\mathbf{r}_i - \mathbf{r}_j|}k^{d-1}dk}{k^\alpha} = c_3\frac{T}{J}\frac{1}{|\mathbf{r}_i - \mathbf{r}_j|^{d-\alpha}} \tag{4.30}$$

for $\alpha < d < \alpha + 1$. Here, c_3 is a dimensionless coefficient,

$$c_3 = 2\frac{C_d}{c_2}\sin\left(-\frac{\pi(d-\alpha-1)}{2}\right)\Gamma(d-\alpha) \tag{4.31}$$

For the case with $d = 1$ and $\alpha = 0.48$, for example, the spin correlation $\langle \sigma_i^x \sigma_j^x \rangle \propto 1/|\mathbf{r}_i - \mathbf{r}_j|^{0.52}$ falls of as a power-law with a smaller power than that in the interaction in the model.

In the strongly interacting phase, the renormalized coupling constant grows at long wavelength and approaches infinity at a characteristic energy scale. In this case, the self-energy correction is large, and the spin correlation function approaches zero.

for the weak coupling along the z-direction, $\Delta < \Delta_c$, the spin correlation falls off as a power-law, $\langle \sigma_i^x \sigma_j^x \rangle \propto 1/|\mathbf{r}_i - \mathbf{r}_j|^{d-\alpha}$, which corresponding to the free magnon phase in Fig. 4.3. For the coupling along z-direction $\Delta > \Delta_c$, the spins are strongly correlated in the z-direction, and uncorrelated along the x-direction $\langle \sigma_i^x \sigma_j^x \rangle = 0$ for $i \neq j$. This corresponds to the strongly interacting phase in Fig. 4.3.

4.4 Relation to non-Anderson disorder-driven transitions

The phase transition we study in this chapter is similar to a completely different type of phase transition — the non-Anderson disorder-driven transitions discussed in Sec. 1.3 for disordered non-interacting semiconductors and semimetals with power-law dispersion $\xi_{\mathbf{k}} \propto k^\alpha$. This similarity is predicted by the interaction-disorder duality introduced in Chap. 2.

The duality maps the phase transition of power-law dispersing bosons at high temperatures studied in this paper to disordered systems with a dimensional reduction of the $d+1$-st dimension, where the dynamics along the extra dimension is approximated by the zero modes. Therefore, the Hamiltonian of the disordered system is effectively

equal to

$$\hat{h} = \hat{\sigma}_z \xi_{\mathbf{k}} + \hat{\sigma}_z u(\boldsymbol{\rho}). \tag{4.32}$$

However, the interacting system considered in this paper does not satisfy the prerequisite of duality mapping because the screening of the interactions is not negligible. Therefore, it is not guaranteed that the two phase transitions belong to the same universality class.

The RG analysis of Eq. (4.32) has been carried out in Ref. [24, 25, 28], and the RG equations can be written as follows

$$\partial_\ell \gamma = (2\alpha - d)\gamma - \gamma^2 \,, \quad \partial_\ell \lambda = \frac{1}{4}\gamma\lambda. \tag{4.33}$$

Here, γ is the dimensionless coupling constant characterizing disorder strength, and λ is the renormalization of energy. These RG equations are similar to the RG equations we derived in this paper Eq. 4.4, but with a numerical difference in the equation of λ, as expected. Hence, the phase transition derived in this paper and the non-Anderson disorder-driven phase transition share the same lower critical dimension but differ in values of the critical exponents, therefore, do not belong to the same universality class.

Chapter 5

Effects of vacancy defects in magnetic materials

This chapter is devoted to the effects of quenched disorder in magnetic materials. Quenched disorder, such as magnetic impurities, vacancies, and lattice defects, are not only inevitable in real materials but also lead to interesting and profound phenomena that cannot be understood in pure materials. This chapter focuses on one such effect, namely the quasispins of vacancy defects.

Vacancy defects, i.e., non-magnetic impurities, are the most common type of quenched disorder in magnetic materials. Though it is caused by a substitution of non-magnetic ions in the magnetic material, the screening of the surrounding magnetic ions can result in a non-zero magnetic moment associated with the vacancy. In a sense, the spin vacancy behaves like a free spin on its own, hence the name "quasispin".

The quasispins of vacancy defects can lead to drastic effects on the magnetic

susceptibility at low temperatures. The susceptibility of the bulk spins satisfies the Curie-Weiss law, $\chi \propto \frac{1}{T+\theta_W}$, where θ_W is the Weiss constant ($\theta_W > 0$ for antiferromagnets), whereas the quasispins give a Curie-like correction ($\propto 1/T$) to the susceptibility [52, 53], which grows faster at low temperatures and can dominant the susceptibility.

In what follows, I will first introduce the effects of vacancy defects in geometrically frustrated (GF) magnets (Sec. 5.1), which motivated us to theoretically study the quasispin effects of vacancies by exactly solving a simple model — 1-dimensional Ising model with nearest-neighbor (NN) and next-to-nearest-neighbor (NNN) interactions (Sec. 5.2). Then I will consider induced interactions between the quasispins due to the bulk spins in between the vacancies (Sec. 5.3).

5.1 Background

Recent works [54, 55] have analyzed the experimental data for the magnetic susceptibility and the glass transition temperature for many GF magnets with different vacancy densities and found an interesting trend. With an increase in the vacancy density in the material, the glass transition temperature decreases, and the magnetic susceptibility increases. The dependence of the glass transition temperature on the vacancy density is as shown in Fig. 5.1.

The increase of the magnetic susceptibility with the increase of vacancy density is counterintuitive. Since the vacancy defects are non-magnetic, increasing vacancy density decreases the density of magnetic ions and therefore, should lead to smaller magnetic susceptibility. However, the experimental data shows the opposite trend. In

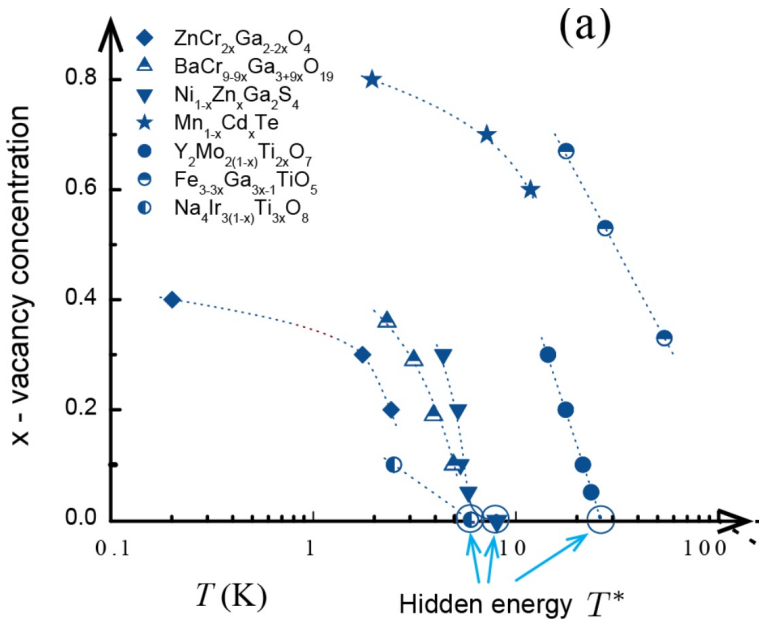

Figure 5.1: Plot taken from Ref. [54], Figure. 2a. The dependence of glass transition temperature on the vacancy densities for available experimental data for GF magnets.

addition, the dependence of the glass transition temperature on the vacancy density is also surprising, as it suggests a hidden energy scale T^* at which a transition to short-range order takes place even for frustrated magnets free of vacancy defects. Moreover, in most of the materials shown in Fig. 5.1, spin vacancies are the only significant source of impurities. Therefore, the transition to short-range order cannot be simply attributed to the quenched disorder in the system. The transition to short-range order in clean frustrated magnets puts the existence of quantum spin liquid in GF magnets in question.

In the following sections, I will focus on explaining the dependence of the magnetic susceptibility on the vacancy density, which can be explained by the "quasispin" of the vacancy defect. The screening of the surrounding spins to the vacancy can introduce a non-zero magnetic moment to the vacancy, which behaves as a free spin, and

contribute a Curie-like term to the magnetic susceptibility, $\chi \propto 1/T$ [52, 53]. Therefore, the magnetic susceptibility for frustrated magnets can be expected to obey the formula [55]:

$$\chi(T) = \frac{A(n - n_{\text{imp}})}{T + \theta_W} + \frac{B n_{\text{imp}}}{T} \tag{5.1}$$

where the first term is the contribution from the bulk spins, which follow the Curie-Weiss law, with θ_W being the Weiss temperature; n_{imp} is the number of vacancies. At low temperatures, the second term grows much faster than the first term. The first term decreases with increasing n_{imp}, but the second term increases with it. So overall, the magnetic susceptibility grows with increasing vacancy density.

In the following sections, I will present a microscopic one-dimensional model, which allows us to derive the quasispin of the vacancies directly.

5.2 Quasispins of vacancy defects in Ising chains with nearest- and next-to-nearest-neighbor interactions

The content of this section were obtained in Ref. [56].

Motivated by the quasispin of vacancies in geometrically frustrated magnets, this section presents an exactly solvable model where one can compute the quasispin of the vacancy defect analytically. The model is the one-dimensional Ising model with NN and NNN interactions, described by the Hamiltonian

$$\hat{H} = J_1 \sum_i \sigma_i \sigma_{i+1} + J_2 \sum_i \sigma_i \sigma_{i+2}, \tag{5.2}$$

where $\sigma_i = \pm 1$ describing the spin-up and spin-down states. This section considers

sufficiently fast decaying interaction, $|J_1/J_2| > 2$, where the NN interaction determines the ground state of the chain; and low temperatures, which are sufficiently smaller than the characteristic energy scale of the system, $T \ll 2|J_1| - 4J_2, |J_2|$. All four cases of ferromagnetic and antiferromagnetic NN and NNN interactions are considered, and the results for each case will be discussed in the subsections below.

5.2.1 Summary of results

The magnetic susceptibilities of an Ising chain with dilute vacancies are given by the formula

$$\chi(T) = \frac{\langle S^2 \rangle}{T} n_{\text{imp}} + \frac{N - b(T) n_{\text{imp}}}{N} \chi_0(T), \tag{5.3}$$

where $\chi_0(T)$ is the susceptibility of a vacancy-free chain, n_{imp} is the number of vacancies, and N is the length of the Ising chain. The formula shows that the effect of vacancies is two-fold:

1. it acts like a free spin of magnitude $\sqrt{\langle S^2 \rangle}$;

2. it effectively reduces the length of the chain by an effective "vacancy size" $b(T)$.

The results for all four cases of chains with ferromagnetic and antiferromagnetic NN and NNN interactions are summarized in Table. 5.1.

For vacancy-free chains with antiferromagnetic NN interactions, the susceptibility $\chi_0(T)$ is exponentially suppressed and non-singular at $T = 0$. As a result, the contribution of quasispins dominants the magnetic susceptibility Eq. (5.3). We find that

NNN \ NN	Antiferromagnetic ($J_1 > 0$)	Ferromagnetic ($J_1 < 0$)
Antiferromagnetic ($J_2 > 0$)	Quasispin $\langle S^2 \rangle = 0$; length increased by $-b \approx e^{(2J_1 - 6J_2)/T}$	Length reduced by $b \approx e^{(2\|J_1\| - 4J_2)/T}$
Ferromagnetic ($J_2 < 0$)	Quasispin $\langle S^2 \rangle = 1$; length reduced by $b \approx e^{(2J_1 - 2J_2)/T}$	Length reduced by $b \approx e^{(2\|J_1\| - 2J_2)/T}$

Table 5.1: The leading effects of a single vacancy on an Ising chain with the NN coupling J_1 and NNN coupling J_2. The vacancy effectively reduces the length of the chain by the "size" $b(T)$. In addition to that, in chains with antiferromagnetic NN interactions and ferromagnetic NNN interactions, a quasipsin is associated with the vacancy.

the quasispin for chains with ferromagnetic and antiferromagnetic NNN interactions are $\langle S^2 \rangle = 1$ and 0, respectively.

For chains with ferromagnetic NN interactions, however, the susceptibility $\chi_0(T)$ of a vacancy free chain is exponentially large at $T \to 0$ and more singular than the quasispin contribution. Therefore, the quasispins are insignificant in this regime.

5.2.2 Qualitative interpretation

Before delving into the details of computing the magnetic susceptibilities, I will first provide a qualitative explanation of the results of the quasispin values. An infinite chain with a vacancy is equivalent to two half-infinite chains whose open ends are coupled by the NNN interaction at the vacancy. As computed in Ref. [56], each end of the half-infinite chain have a magnetic moment of 1/2. When the two ends are

coupled by ferromagetic NNN interaction, the magnetic moments add up and resulting in the magnetic moment $\langle S^2 \rangle = 1$ of the vacancy; while when the two ends are coupled by antiferromagnetic NNN interaction, the magnetic moments anti-align and resulting in a zero magnetic moment of the vacancy.

5.2.3 Computation of the magnetic susceptibility

The contribution of the vacancy to the magnetic susceptibility is computed by directly computing the magnetic susceptibility for a chain with and without a vacancy, as shown in Fig. 5.2. The magnetic susceptibility can be computed using the fluctuation-dissipation theorem, which is given by

$$\chi(T) = \frac{\langle M^2 \rangle}{T} = \frac{1}{T} \sum_{i,j} \langle \sigma_i \sigma_j \rangle, \tag{5.4}$$

where $M = \sum_i \sigma_i$ is the total magnetisation of the system; $\langle \ldots \rangle$ is averaging with respect to the thermal state of the system at temperature T; and the summation with respect to the indices i and j runs over all sites with spins. Here, we have used that the average magnetization is zero for Ising chains without external fields.

The spin correlation functions can be computed using the domain-wall-gas approximation, which maps the Ising chain to a one-dimensional ideal gas of domain walls. This approximation is accurate when the domain wall excitations are dilute, which is in accordance with the aforementioned low-temperature regime, $T \ll 2|J_1| - 4J_2, |J_2|$, considered in this chapter. The density of single domain walls is given by $n_D \approx \exp(E_D/T) \ll 1$, while the density of 2π-domain walls (i.e., two domain walls on neighboring sites) is given by $n_{DD} \approx n_D \exp(-2|J_1|/T) \ll n_D$. Therefore, the domain

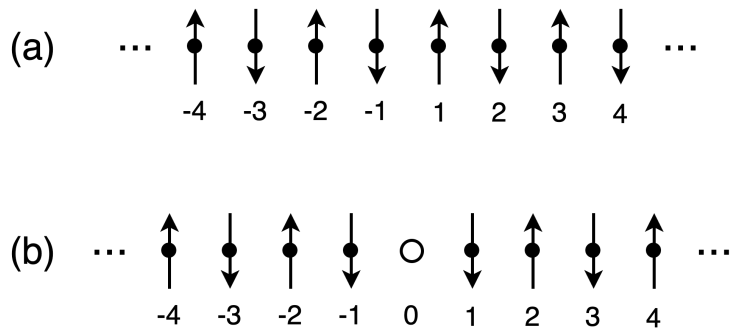

Figure 5.2: Spin configurations in the ground states of Ising chains with antiferromagnetic NN interactions and ferromagnetic NNN interactions. (a) A chain without a vacancy. (b) A chain with a vacancy.

walls are dilute, and the approximation to an ideal gas is justified.

The domain-wall-gas approximation allows us to compute the spin correlation function in Eq. (5.4). I present the results of the spin correlations here, and the details of the derivation for a chain with antiferromagnetic NN interactions are given in the subsection immediately follows.

The spin correlations for a chain without vacancy are given by

$$\langle \sigma_i \sigma_j \rangle_0 = \pm \frac{1 - e^{-\beta E_D}}{1 + e^{-\beta E_D}}, \tag{5.5}$$

where "+" and "−" signs for ferromagnetic and antiferromagnetic NN interactions, respectively; and $E_D = 2|J_1| - 4J_2$ is the energy of the domain walls. Utilizing Eq. (5.4), the magnetic susceptibility for a chain without a vacancy can be derived and is given by

$$\chi_0(T) \approx N T^{-1} e^{\mp E_D/T}. \tag{5.6}$$

Here, N is the length of the chain, and "+" and "−" signs are for ferromagnetic and antiferromagnetic NN interactions, respectively.

The spin correlations for a chain with a vacancy, as shown in Fig. 5.2b, for the case with antiferromagnetic NN and ferromagnetic NNN interactions are derived in Sec. 5.2.4 and are given by

$$\langle \sigma_{-1}\sigma_1 \rangle = \frac{1 - e^{2\beta J_2}}{1 + e^{2\beta J_2}}, \tag{5.7a}$$

$$\langle \sigma_1\sigma_j \rangle \approx \frac{e^{-\beta E_D - 2\beta J_2} - 1}{1 + e^{-\beta E_D - 2\beta J_2}} \left(\frac{e^{-\beta E_D} - 1}{1 + e^{-\beta E_D}} \right)^{j-2}, \tag{5.7b}$$

$$\langle \sigma_{-1}\sigma_j \rangle \approx \langle \sigma_{-1}\sigma_1 \rangle \langle \sigma_1\sigma_j \rangle, \tag{5.7c}$$

$$\langle \sigma_i\sigma_j \rangle \approx \langle \sigma_i\sigma_{-1} \rangle \langle \sigma_{-1}\sigma_1 \rangle \langle \sigma_1\sigma_j \rangle, \tag{5.7d}$$

for $i \leq -2$ and $j \geq 2$. Because of the symmetry of the chain, the correlators satisfy the following relation for all i and j

$$\langle \sigma_i\sigma_j \rangle = \langle \sigma_{-i}\sigma_{-j} \rangle. \tag{5.8}$$

The contribution of one vacancy to the susceptibility can be computed using Eq. (5.4) and is given by the difference between the susceptibility of a chain with and without a vacancy

$$\begin{aligned} \chi(T) - \chi_0(T) = {} & 2\beta \left(\langle \sigma_{-1}\sigma_1 \rangle - \langle \sigma_{-1}\sigma_1 \rangle_0 \right) + 4\beta \sum_{j=2}^{+\infty} \left(\langle \sigma_1\sigma_j \rangle - \langle \sigma_1\sigma_j \rangle_0 \right) \\ & + 4\beta \sum_{j=2}^{+\infty} \left(\langle \sigma_{-1}\sigma_j \rangle - \langle \sigma_{-1}\sigma_j \rangle_0 \right) + 2\beta \sum_{i=-2}^{-\infty} \sum_{j=2}^{+\infty} \left(\langle \sigma_i\sigma_j \rangle - \langle \sigma_i\sigma_j \rangle_0 \right). \end{aligned} \tag{5.9}$$

Here, the magnetic susceptibility χ and the correlation $\langle \cdots \rangle$ are for a chain with a vacancy, χ_0 and $\langle \cdots \rangle_0$ are for a chain without vacancies, the labels of the chains with and without a vacancy are given in Fig. 5.2.

For antiferromagnetic NN interactions ($J_1 > 0$), Eqs. (5.7a)-(5.7d) and (5.4)

give the vacancy contribution to the magnetic susceptibilities

$$\chi(T) - \chi_0(T) = T^{-1} - T^{-1}e^{-2|J_2|/T} + o\left(T^{-1}e^{-2|J_2|/T}\right), \tag{5.10}$$

for a chain with ferromagnetic NNN interactions ($J_2 < 0$), and

$$\chi(T) - \chi_0(T) = T^{-1}e^{-2|J_2|/T} + o\left(T^{-1}e^{-2|J_2|/T}\right), \tag{5.11}$$

for a chain with antiferromagnetic NNN interactions ($J_2 > 0$). In accordance with Eq. (5.3), the first term is the quasispin contribution with $\langle S^2 \rangle = 1$, and the second term describes an effective length reduction of the chain by effective vacancy sizes $b(T) \approx e^{(2J_1-2J_2)/T}$ for ferromagnetic NNN interactions. For antiferromagnetic NNN interactions, (5.11) corresponds to a quasispin $\langle S^2 \rangle = 0$ and an effective length increase by $-b(T) \approx -e^{(2J_1-2J_2)/T}$.

The case with ferromagnetic NN interactions can be computed similarly, and the details of the calculations of the spin correlations and the magnetic susceptibilities are given in Ref. [56]. The results for the leading effects of the vacancy on the susceptibility are summarised in Table 5.1.

5.2.4 Details of calculations for chains with antiferromagnetic NN interactions

In this subsection, I provide the details of the derivation of the vacancy contributions to the susceptibilities for chains with antiferromagnetic NN interactions. The calculation is similar for chains with ferromagnetic NN interactions, and is provided in Ref. [56].

In the ground state of a chain with antiferromagnetic NN interactions, neighboring spins are antiparallel. Each excited state can be considered as a sequence of domain walls, i.e., pairs of neighboring parallel spins separating antiferromagnetic domains. Spin correlations can be found by mapping the chain to a gas of domain walls.

In a system of size r, the partition function of the domain-wall excitations is given by

$$Z = 1 + C_r^1 e^{-\beta E_D} + \left(C_r^2 - C_{r-1}^1\right) e^{-2\beta E_D} + C_{r-1}^1 e^{-2\beta E_D - 4\beta J_2} + \cdots , \tag{5.12}$$

where

$$E_D = 2J_1 - 4J_2 \tag{5.13}$$

is the energy of a single domain wall and $C_n^k = \frac{n!}{k!(n-k)!}$ is the binomial coefficient. The second term on the right-hand side of Eq. (5.12) is the contribution of a single domain wall, and the third term comes from two domain walls that are not located next to each other, with $C_r^2 - C_{r-1}^1$ being the number of such configurations. The fourth term comes from two domain walls next to each other.

In the limit of low temperatures, $T \ll E_D, |J_2|$, the domain-wall excitations are very sparse, and the system can be considered as an ideal gas of domain walls. In this limit, configurations with domain walls located next to each other can be neglected. The spin correlations $\langle \sigma_i \sigma_j \rangle$ can be found by counting the domain walls in between the two spins σ_i and σ_j, and is given by

$$\langle \sigma_i \sigma_j \rangle_0 \approx (-1)^r \, \frac{1 - C_r^1 e^{-\beta E_D} + C_r^2 e^{-2\beta E_D} - \cdots}{1 + C_r^1 e^{-\beta E_D} + C_r^2 e^{-2\beta E_D} + \cdots} = \left(\frac{e^{-\beta E_D} - 1}{1 + e^{-\beta E_D}} \right)^r , \tag{5.14}$$

where $r = |i - j|$. According to this equation, the correlation length in the spin chain is given by

$$\xi \approx \left[\log\left(\frac{1+e^{-\beta E_D}}{1-e^{-\beta E_D}}\right)\right]^{-1} \approx \frac{1}{2}e^{\beta E_D}. \tag{5.15}$$

In this paper, we assume that the length of the chain N is much longer than the correlation length ξ.

Equation (5.14) together with the fluctuation-dissipation relation (5.4) give the magnetic susceptibility for a chain without vacancies

$$\chi_0(T) = \beta \sum_{i,j} \langle \sigma_i \sigma_j \rangle_0 \approx \beta N + 2\beta N \, \frac{e^{-\beta E_D} - 1}{1 + e^{-\beta E_D}} \left(1 - \frac{e^{-\beta E_D} - 1}{1 + e^{-\beta E_D}}\right)^{-1} = \beta N e^{-\beta E_D}. \tag{5.16}$$

The spin correlations for a chain with a vacancy can be similarly computed by mapping the chain to an ideal gas of domain walls. For chains with antiferromagnetic NN and ferromagnetic NNN interactions, the ground state spin configuration in the chain with the vacancy is as shown in Fig. 5.2b; for chains with antiferromagnetic NNN interactions, the ground state spin configuration is given by flipping half of the chain in Fig. 5.2b on one side of the vacancy. The presence of the vacancy modifies the domain-wall energies near and at the vacancy.

For both ferromagnetic and antiferromagnetic NNN interactions, the domain wall at the location of the vacancy, i.e. in between sites -1 and 1, has an energy of $2|J_2|$. A domain-wall excitation between sites 1 and 2 or between sites -1 and -2 has an energy of $2J_1 - 2J_2$, and the energy of domain walls at the other locations is unchanged by the vacancy, $E_D = 2J_1 - 4J_2$. Using these excitation energies, we obtain

the correlators of spins in the chain with a vacancy:

$$\langle\sigma_{-1}\sigma_1\rangle = \pm\frac{1-e^{2\beta J_2}}{1+e^{2\beta J_2}}, \tag{5.17a}$$

$$\langle\sigma_1\sigma_j\rangle \approx \frac{e^{-2\beta J_1+2\beta J_2}-1}{1+e^{-2\beta J_1+2\beta J_2}}\left(\frac{e^{-\beta E_D}-1}{1+e^{-\beta E_D}}\right)^{j-2}, \tag{5.17b}$$

$$\langle\sigma_{-1}\sigma_j\rangle \approx \pm\frac{1-e^{2\beta J_2}}{1+e^{2\beta J_2}}\,\frac{e^{-2\beta J_1+2\beta J_2}-1}{1+e^{-2\beta J_1+2\beta J_2}}\left(\frac{e^{-\beta E_D}-1}{1+e^{-\beta E_D}}\right)^{j-2}, \tag{5.17c}$$

$$\langle\sigma_i\sigma_j\rangle \approx \pm\frac{1-e^{2\beta J_2}}{1+e^{2\beta J_2}}\left(\frac{e^{-2\beta J_1+2\beta J_2}-1}{1+e^{-2\beta J_1+2\beta J_2}}\right)^2\left(\frac{e^{-\beta E_D}-1}{1+e^{-\beta E_D}}\right)^{j-i-4}, \tag{5.17d}$$

for $i \leq -2$, $j \geq 2$. Here, "+" and "−" signs corresponds to ferromagnetic and antiferromagnetic NNN interactions, respectively. For $i, j \leq -2$ and $i, j \geq 2$, the correlators are unaltered by the presence of the vacancy and are given by Eq. (5.14). All the correlators satisfy the symmetry relation $\langle\sigma_i\sigma_j\rangle = \langle\sigma_{-i}\sigma_{-j}\rangle$.

The magnetic susceptibility of the vacancy is given by the difference in the susceptibilities of the chain with and without the vacancy, as is given in Eq. (5.9). The correlators for a vacancy-free chain given by Eq. (5.14) can be rewritten in terms of the chosen labels as shown in Fig. 5.2,

$$\langle\sigma_i\sigma_j\rangle_0 \approx \left(\frac{e^{-\beta E_D}-1}{1+e^{-\beta E_D}}\right)^{j-i-1}, \quad \text{for } i \leq -1,\ j \geq 1; \tag{5.18a}$$

$$\langle\sigma_i\sigma_j\rangle_0 \approx \left(\frac{e^{-\beta E_D}-1}{1+e^{-\beta E_D}}\right)^{|j-i|}, \quad \text{for } i, j \leq -1 \text{ and } i, j \geq 1. \tag{5.18b}$$

Utilising Eqs. (5.17a)-(5.17d), (5.18a)-(5.18b) and (5.9), one can obtain the

magnetic susceptibility of the vacancy

$$\chi(T)-\chi_0(T)\approx 2\beta\left(\frac{1-e^{2\beta J_2}}{1+e^{2\beta J_2}}-\frac{e^{-\beta E_D}-1}{1+e^{-\beta E_D}}\right) + 4\beta\left(\frac{1}{1+e^{2\beta J_2}}\frac{e^{-2\beta J_1+2\beta J_2}-1}{1+e^{-2\beta J_1+2\beta J_2}}-\frac{e^{-\beta E_D}}{1+e^{-\beta E_D}}\frac{e^{-\beta E_D}-1}{1+e^{-\beta E_D}}\right)\left(1+e^{-\beta E_D}\right) + \frac{\beta}{2}\left[\frac{1-e^{2\beta J_2}}{1+e^{2\beta J_2}}\left(\frac{e^{-2\beta J_1+2\beta J_2}-1}{1+e^{-2\beta J_1+2\beta J_2}}\right)^2-\left(\frac{e^{-\beta E_D}-1}{1+e^{-\beta E_D}}\right)^3\right]\left(1+e^{-\beta E_D}\right)^2 \tag{5.19}$$

for ferromagnetic NNN interactions; and

$$\chi(T)-\chi_0(T)\approx 2\beta\left(\frac{e^{-2\beta J_2}-1}{1+e^{-2\beta J_2}}-\frac{e^{-\beta E_D}-1}{1+e^{-\beta E_D}}\right) + 4\beta\left(\frac{e^{-2\beta J_2}}{1+e^{-2\beta J_2}}\frac{e^{-2\beta J_1+2\beta J_2}-1}{1+e^{-2\beta J_1+2\beta J_2}}-\frac{e^{-\beta E_D}}{1+e^{-\beta E_D}}\frac{e^{-\beta E_D}-1}{1+e^{-\beta E_D}}\right)\left(1+e^{-\beta E_D}\right) + \frac{\beta}{2}\left[\frac{e^{-2\beta J_2}-1}{1+e^{-2\beta J_2}}\left(\frac{e^{-2\beta J_1+2\beta J_2}-1}{1+e^{-2\beta J_1+2\beta J_2}}\right)^2-\left(\frac{e^{-\beta E_D}-1}{1+e^{-\beta E_D}}\right)^3\right]\left(1+e^{-\beta E_D}\right)^2 \tag{5.20}$$

for antiferromagnetic NNN interactions.

At low temperatures, $T \ll E_D$, $|J_2|$, these give the results of the vacancy's susceptibilities Eqs. (5.10) and (5.11) for ferromagnetic and antiferromagnetic NNN interactions.

5.3 Emergent interactions between quasispins

The results of this section were obtain in Ref. [57].

Section. 5.2 has focused on dilute vacancy defects (i.e., the distance between vacancies much larger than the correlation length ξ), where one can consider the vacancies independently. For a chain with a finite density of vacancies, however, vacancies can

be correlated with one another through the bulk spins in between the two vacancies. Such correlation can give a correction to the magnetic susceptibility of a chain with vacancies, which grows fast with vacancy densities. This section computes the correlations between the vacancies for Ising chains with antiferromagnetic NN interactions and ferromagnetic NNN interactions, described by the Hamiltonian Eq. (5.2), with $J_1 > 0$, $J_2 < 0$, which is the case with quasispin $\langle S^2 \rangle = 1$ as is derived in the previous section.

5.3.1 Summary of results

In the limit of low temperatures, the correlation function of two quasispins of vacancies with distance ℓ apart is given by

$$\langle S_1 S_2 \rangle = (-1)^{\ell} \exp\left(-|\ell|/\xi\right), \tag{5.21}$$

where ξ is the correlation length in the clean system, Eq. (5.15). This matches with the correlation function between spins in a vacancy-free system. Such quasispin correlation leads to a correction to the magnetic susceptibility $\chi(T)$ of a chain with a finite density of vacancies.

$$\chi(T) \approx \frac{n_{\text{imp}}}{T} \left\{ 1 - \frac{1}{2} \frac{n_{\text{imp}}}{N} + \mathcal{O}\left[\left(\frac{n_{\text{imp}}}{N} \right)^2 \right] \right\} + \chi_{\text{bulk}}(T) \tag{5.22}$$

Here, χ_{bulk} describes the contribution to the magnetic susceptibility from the bulk spins,

$$\chi_{\text{bulk}}(T) = \frac{N - b(T) n_{\text{imp}}}{N} \chi_0(T), \tag{5.23}$$

where $\chi_0(T)$ is again the susceptibility of the vacancy-free chain and $b(T)$ is the vacancy size given in the bottom left cell of Table. 5.1. The second term in Eq. (5.22) follows

from the first virial correction to the susceptibility, which accounts for the effects of the quasispin correlation to the leading order.

5.3.2 The magnetic susceptibility for two vacancies

We derive the correlations between quasispins by explicitly computing the magnetic susceptibility of a chain with two vacancies and comparing it with a chain without vacancies, as shown in Fig. 5.3. Without loss of generality, we assume the two vacancies are located at sites 0 and ℓ.

The magnetic susceptibility of the chain is computed similarly to the previous section, with the difference between the susceptibilities for chains with and without vacancies given by

$$\begin{aligned}\chi(T) - \chi_0(T) = 4\beta \sum_{i=2}^{\ell-2} \sum_{j=\ell-1}^{\infty} (\langle \sigma_i \sigma_j \rangle - \langle \sigma_i \sigma_j \rangle_0) + 4\beta \sum_{j=\ell+1}^{\infty} (\langle \sigma_{\ell-1} \sigma_j \rangle - \langle \sigma_{\ell-1} \sigma_j \rangle_0) \\ + 4\beta \sum_{j=\ell+2}^{\infty} (\langle \sigma_{\ell+1} \sigma_j \rangle - \langle \sigma_{\ell+1} \sigma_j \rangle_0) + 2\beta \sum_{i=-\infty}^{1} \sum_{j=\ell-1}^{\infty} (\langle \sigma_i \sigma_j \rangle - \langle \sigma_i \sigma_j \rangle_0)\end{aligned} \tag{5.24}$$

where χ and χ_0 are the susceptibilities for chains with and without the two vacancies, as shown in Fig. 5.3 (a) and (b), respectively. In each of the sums, we extend the upper limits to infinity. This is a good approximation so long as the locations of the vacancies are sufficiently far away from the chain ends, i.e., the distance is much larger than the correlation length ξ.

The spin correlators and the magnetic susceptibilities are computed using the same method presented in the previous section. Therefore, in this section, I only report

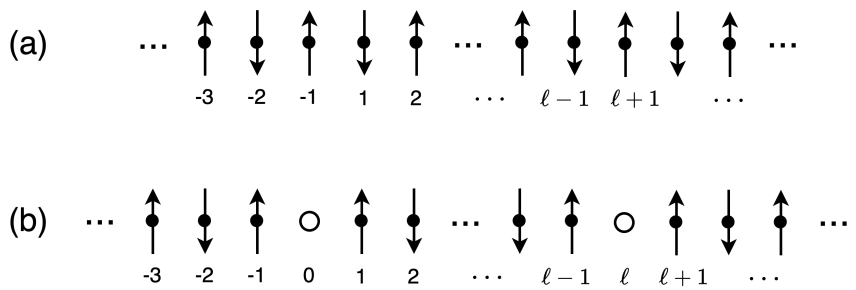

Figure 5.3: Spin configurations in the ground states of Ising chains with antiferromagnetic NN interactions and ferromagnetic NNN interactions (a) without vacancies (b) with two vacancies of distance ℓ apart.

the results. The details of the calculations are given in Ref. [57].

The difference in the magnetic susceptibilities of chains with and without the two vacancies depends on the distance ℓ and is equal to

$$\chi - \chi_0 \approx \frac{2}{T}\left[1+(-1)^{\ell}e^{-|\ell|/\xi}\right] - \left[1+2(-1)^{\ell}e^{-|\ell|/\xi}\right]T^{-1}e^{-2|J_2|/T} + \mathcal{O}\left(T^{-1}e^{-2J_1/T}\right) \tag{5.25}$$

for $|\ell| \geq 2$. For $|\ell| = 1$, i.e. for the vacancies neighbouring each other, the two vacancies break the chain into two independent semi-infinite chains. The susceptibility of such a system is given by

$$\chi \approx \frac{1}{2T} + \chi_0 + \mathcal{O}\left(T^{-1}e^{-(2J_1+2|J_2|)/T}\right). \tag{5.26}$$

The two free ends each contributes a quasispin $\sqrt{\langle S^2\rangle} = \frac{1}{2}$, giving the first term in the above magnetic susceptibility.

5.3.3 Correlation between quasispins

To obtain the correlation between quasispins, we note that the susceptibility differences computed in the previous subsection can be derived from a quasispin picture,

following the fluctuation-dissipation theorem for the quasispins.

$$\chi(T) = \frac{2}{T} + \frac{2\langle S_1 S_2 \rangle}{T} + \chi_{\rm bulk}(T), \tag{5.27}$$

where the first term describes the contribution of two isolated quasispins, $\langle S^2 \rangle = 1$; $\langle S_1 S_2 \rangle$ is the correlator of the quasispins of the two vacancies; and $\chi_{\rm bulk}(T) \approx \chi_0(T) - 2T^{-1}e^{-2|J_2|/T} = \left[1 - \frac{2}{N}b(T)\right]\chi_0(T)$.

Comparing Eq. (5.27) with the results of the susceptibility difference between chains with and without vacancies in the precious section, Eqs. (5.25) and (5.26), we can derive the quasispin correlations. For two vacancies with distance ℓ apart, the correlation function is given by

$$\langle S_1 S_2 \rangle \approx (-1)^{\ell} \exp\left(-\frac{|\ell|}{\xi}\right) + \mathcal{O}\left(T^{-1}e^{-2|J_2|/T}\right), \tag{5.28}$$

for $|\ell| \geq 2$, and

$$\langle S_1 S_2 \rangle \approx -\frac{3}{4} + \mathcal{O}\left(T^{-1}e^{-2|J_2|/T}\right), \tag{5.29}$$

for two adjacent vacancies. These expressions assume the translational invariance of the vacancy locations, which is fulfilled so long as the vacancies are sufficiently far away from the chain ends, i.e., much larger than the correlation length.

5.3.4 First virial correction to the susceptibility

The magnetic susceptibility for a chain with $n_{\rm imp}$ randomly located vacancies is given by

$$\chi(T) = \frac{n_{\rm imp}}{T} + \frac{1}{T}\sum_{\substack{\alpha\neq\beta,\\ \alpha,\beta=1}}^{n_{\rm imp}} \langle\langle S_\alpha S_\beta \rangle\rangle_{\rm loc} + \chi_{\rm bulk}(T). \tag{5.30}$$

This again follows directly from the fluctuation-dissipation theorem for the quasispins. Here, $\langle S_\alpha S_\beta \rangle$ is the correlator of quasispins α and β and

$$\langle \ldots \rangle_{\rm loc} = \frac{1}{N^{N_{\rm vac}}} \sum_{x_1=1}^{N} \sum_{x_2=1}^{N} \cdots \sum_{x_{n_{\rm imp}}=1}^{N} \ldots$$

is averaging with respect to the locations x_1, x_2, ..., $x_{n_{\rm imp}}$ of the vacancies. We consider large numbers $N_{vac} \gg 1$ and dilute densities of vacancies. The dilute limit is taken such that one can expand the correction due to vacancy correlations to the susceptibility up to the first virial order, i.e., consider only configurations with one pair of vacancies within a distance of order correlation length apart $\ell \sim \xi$, and all other vacancies to be much further away $\ell \gg \xi$. Then, the summation in the above expression can be approximated as

$$\chi(T) \approx \frac{n_{\rm imp}\langle S^2 \rangle}{T} + 2\frac{n_{\rm imp}^2}{N} \sum_{\ell=1}^{\infty} \frac{\langle S_i S_{i+\ell} \rangle}{T} + \chi_{\rm bulk}(T). \tag{5.31}$$

Substituting the results of the correlators Eqs. (5.28) and (5.29) to this formula and carrying out the sum, we get

$$\chi(T) = \frac{n_{\rm imp}}{T} - \frac{n_{\rm imp}^2}{2NT} + \mathcal{O}\left[\left(\frac{n_{\rm imp}}{N}\right)^2\right] + \chi_{\rm bulk}(T) \tag{5.32}$$

for the susceptibility of $n_{\rm imp}$ randomly located vacancies in the dilute limit. The next order correction is of order $n_{\rm imp}/N$ smaller.

Chapter 6

Conclusion

In this thesis, I start by presenting an equivalence between a broad class of interacting disorder-free and disordered non-interacting systems. I present a careful derivation of the duality which is valid to all orders in perturbation theory. I then use duality mapping to predict three unconventional phase transitions by mapping existing ones to them. The first two examples are disorder-driven transitions that expanded the classes of non-Anderson disorder-driven transitions introduced by previous works [19, 24, 25]. The disorder-driven transitions are disorder-driven transitions in nodal-point semimetal and nodal-line semimetal, dual to the BCS-BEC crossover and the BCS-superconducting transition, respectively.

The third example is an unconventional interaction-driven transition found by mapping of disorder-driven transitions. Applying a field-theoretical renormalization group analysis, I derive a phase transition for dilute gases of bosons with power-law dispersions. at finite temperatures. I also provide a concrete example that exhibits this

transition — the XXZ model with long-range interactions, with the interaction strength decay as the distance to the power $d + \alpha$. The model can be realized in trapped-ion experiments, and I show that one can detect such phase transition by a measurement of the spin correlation functions. This transition is similar to the non-Anderson disorder-driven transition, which is directly followed from the established interaction-disorder duality.

Finally, in the last chapter, I discussed an interesting effect of spin vacancies in magnetic materials, namely, it can have a "quasispin" degree of freedom, which acts like a free spin in a magnetic field. I derive the quasispin value for Ising chains with nearest- and next-to-nearest-neighbor interactions. Then, I study the effective interactions between the quasispins generated by the correlations of the bulk spins and derive the first virial correction to the magnetic susceptibility for a finite density of vacancies.

Bibliography

[1] P. W. Anderson. Absence of diffusion in certain random lattices. *Phys. Rev.*, 109:1492–1505, Mar 1958.

[2] S F Edwards and P W Anderson. Theory of spin glasses. *Journal of Physics F: Metal Physics*, 5(5):965, may 1975.

[3] G. Parisi and N. Sourlas. Random magnetic fields, supersymmetry, and negative dimensions. *Phys. Rev. Lett.*, 43:744–745, Sep 1979.

[4] K.B. Efetov. Supersymmetry and theory of disordered metals. *Advances in Physics*, 32(1):53–127, 1983.

[5] K. B. Efetov. *Supersymetry in Disorder and Chaos*. Cambridge University Press, New York, 1999.

[6] Julian S. Schwinger. Brownian motion of a quantum oscillator. *J. Math. Phys.*, 2:407–432, 1961.

[7] L. V. Keldysh. Diagram technique for nonequilibrium processes. *Zh. Eksp. Teor. Fiz.*, 47:1515–1527, 1964.

[8] R. P. Feynman and F. L. Vernon, Jr. The Theory of a general quantum system interacting with a linear dissipative system. *Annals Phys.*, 24:118–173, 1963.

[9] Elihu Abrahams. *50 Years of Anderson Localization.* World Scientific, 2010.

[10] Ad Lagendijk, Bart van Tiggelen, and Diederik S. Wiersma. Fifty years of Anderson localization. *Physics Today*, 62(8):24–29, 08 2009.

[11] Chen Guan and Xingyue Guan. A brief introduction to anderson localization. 2019.

[12] Alain Aspect and Massimo Inguscio. Anderson localization of ultracold atoms. *Physics Today*, 62(8):30–35, 08 2009.

[13] N.F. Mott and W.D. Twose. The theory of impurity conduction. *Advances in Physics*, 10(38):107–163, 1961.

[14] V. L. Berezinsky. Destruction of Long-range Order in One-dimensional and Two-dimensional Systems Possessing a Continuous Symmetry Group. II. Quantum Systems. *Sov. Phys. JETP*, 34(3):610, 1972.

[15] D J Thouless. A relation between the density of states and range of localization for one dimensional random systems. *Journal of Physics C: Solid State Physics*, 5(1):77, Jan 1972.

[16] E. Abrahams, P. W. Anderson, D. C. Licciardello, and T. V. Ramakrishnan. Scaling theory of localization: Absence of quantum diffusion in two dimensions. *Phys. Rev. Lett.*, 42:673–676, Mar 1979.

[17] Alexander D. Mirlin. Statistics of energy levels and eigenfunctions in disordered and chaotic systems: Supersymmetry approach. *Arxiv:cond-mat/0006421*, 2000.

[18] P. W. Anderson, D. J. Thouless, E. Abrahams, and D. S. Fisher. New method for a scaling theory of localization. *Phys. Rev. B*, 22:3519–3526, Oct 1980.

[19] S. V. Syzranov and L. Radzihovsky. High-dimensional disorder-driven phenomena in Weyl semimetals, semiconductors, and related systems. *Annu. Rev. Cond. Mat. Phys.*, 9:33–58, 2018.

[20] Eduardo Fradkin. Critical behavior of disordered degenerate semiconductors. I. Models, symmetries, and formalism. *Phys. Rev. B*, 33:3257–3262, 1986.

[21] Eduardo Fradkin. Critical behavior of disordered degenerate semiconductors. II. Spectrum and transport properties in mean-field theory. *Phys. Rev. B*, 33:3263–3268, 1986.

[22] A. Rodríguez, V. A. Malyshev, G. Sierra, M. A. Martín-Delgado, J. Rodríguez-Laguna, and F. Domínguez-Adame. Anderson Transition in Low-Dimensional Disordered Systems Driven by Long-Range Nonrandom Hopping. *Phys. Rev. Lett.*, 90:027404, Jan 2003.

[23] A. V. Malyshev, V. A. Malyshev, and F. Domínguez-Adame. Monitoring the localization-delocalization transition within a one-dimensional model with nonrandom long-range interaction. *Phys. Rev. B*, 70:172202, Nov 2004.

[24] S. V. Syzranov, L. Radzihovsky, and V. Gurarie. Critical Transport in Weakly Disordered Semiconductors and Semimetals. *Phys. Rev. Lett.*, 114:166601, 2015.

[25] S. V. Syzranov, V. Gurarie, and L. Radzihovsky. Unconventional localisation transition in high dimensions. *Phys. Rev. B*, 91:035133, 2015.

[26] T. Louvet, D. Carpentier, and A. A. Fedorenko. On the disorder-driven quantum transition in three-dimensional relativistic metals. *Phys. Rev. B*, 94:220201, Dec 2016.

[27] Bitan Roy, Robert-Jan Slager, and Vladimir Juričić. Global Phase Diagram of a Dirty Weyl Liquid and Emergent Superuniversality. *Phys. Rev. X*, 8:031076, Sep 2018.

[28] S. V. Syzranov, P. M. Ostrovsky, V. Gurarie, and L. Radzihovsky. Critical exponents at the unconventional disorder-driven transition in a Weyl semimetal. *Phys. Rev. B*, 93:155113, Apr 2016.

[29] J. H. Pixley, D. A. Huse, and S. Das Sarma. Rare-Region-Induced Avoided Quantum Criticality in Disordered Three-Dimensional Dirac and Weyl Semimetals. *Physical Review X*, 6(2):021042, April 2016.

[30] Björn Sbierski, Emil J. Bergholtz, and Piet W. Brouwer. Quantum critical exponents for a disordered three-dimensional Weyl node. *Phys. Rev. B*, 92:115145, Sep 2015.

[31] Soumya Bera, Jay D. Sau, and Bitan Roy. Dirty Weyl semimetals: Stability, phase transition, and quantum criticality. *Phys. Rev. B*, 93:201302, May 2016.

[32] B. Sbierski, K. S. C. Decker, and P. W. Brouwer. Weyl node with random vector potential. *Phys. Rev. B*, 94(22):220202, December 2016.

[33] Shang Liu, Tomi Ohtsuki, and Ryuichi Shindou. Effect of disorder in three dimensional layered Chern insulator. *Phys. Rev. Lett.*, 116:066401, 2016.

[34] Ivan Balog, David Carpentier, and Andrei A. Fedorenko. Disorder-Driven Quantum Transition in Relativistic Semimetals: Functional Renormalization via the Porous Medium Equation. *Phys. Rev. Lett.*, 121:166402, 2018.

[35] Xunlong Luo, Baolong Xu, Tomi Ohtsuki, and Ryuichi Shindou. Quantum multicriticality in disordered Weyl semimetals. *Phys. Rev. B*, 97:045129, Jan 2018.

[36] Shijun Sun and Sergey Syzranov. Interactions-disorder duality and critical phenomena in nodal semimetals, dilute gases, and other systems. *Phys. Rev. B*, 108:195132, Nov 2023.

[37] Joshua Feinberg and A. Zee. Non-hermitian random matrix theory: Method of hermitian reduction. *Nuclear Physics B*, 504(3):579–608, 1997.

[38] K. B. Efetov. Quantum disordered systems with a direction. *Phys. Rev. B*, 56:9630–9648, Oct 1997.

[39] Zongping Gong, Yuto Ashida, Kohei Kawabata, Kazuaki Takasan, Sho Hi-

gashikawa, and Masahito Ueda. Topological phases of non-hermitian systems. *Phys. Rev. X*, 8:031079, Sep 2018.

[40] Xunlong Luo, Zhenyu Xiao, Kohei Kawabata, Tomi Ohtsuki, and Ryuichi Shindou. Unifying the anderson transitions in hermitian and non-hermitian systems. *Phys. Rev. Res.*, 4:L022035, May 2022.

[41] A. A. Abrikosov, L. P. Gorkov, and I. E. Dzyaloshinski. *Methods of Quantum Field Theory in Statistical Physics*. Dover, New York, 1975.

[42] A. Altland and B. Simons. *Condensed Matter Field Theory*. Leiden: Cambridge University Press, 2006.

[43] D.I. Uzunov. On the zero temperature critical behaviour of the nonideal Bose gas. *Physics Letters A*, 87(1):11–14, 1981.

[44] V. Gurarie and L. Radzihovsky. Resonantly paired fermionic superfluids. *Annals of Physics*, 322(1):2–119, 2007. January Special Issue 2007.

[45] Predrag Nikolic and Subir Sachdev. Renormalization-group fixed points, universal phase diagram, and $1/N$ expansion for quantum liquids with interactions near the unitarity limit. *Phys. Rev. A*, 75:033608, Mar 2007.

[46] Martin Y. Veillette, Daniel E. Sheehy, and Leo Radzihovsky. Large-N expansion for unitary superfluid Fermi gases. *Phys. Rev. A*, 75:043614, Apr 2007.

[47] Siyu Zhu and Sergey Syzranov. BCS-like disorder-driven instabilities and ultraviolet effects in nodal-line semimetals. *Annals of Physics*, 459:169501, 2023.

[48] R. Islam, C. Senko, W. C. Campbell, S. Korenblit, J. Smith, A. Lee, E. E. Edwards, C.-C. J. Wang, J. K. Freericks, and C. Monroe. Emergence and frustration of magnetism with variable-range interactions in a quantum simulator. *Science*, 340(6132):583–587, May 2013.

[49] Michael Knap, Adrian Kantian, Thierry Giamarchi, Immanuel Bloch, Mikhail D. Lukin, and Eugene Demler. Probing real-space and time-resolved correlation functions with many-body ramsey interferometry. *Physical Review Letters*, 111(14), October 2013.

[50] S. Lepoutre, J. Schachenmayer, L. Gabardos, B. Zhu, B. Naylor, E. Marechal, O. Gorceix, A. M. Rey, L. Vernac, and B. Laburthe-Tolra. Exploring out-of-equilibrium quantum magnetism and thermalization in a spin-3 many-body dipolar lattice system. *Nat. Commun.*, 10(1):1714, 2019.

[51] Lei Feng, Or Katz, Casey Haack, Mohammad Maghrebi, Alexey V. Gorshkov, Zhexuan Gong, Marko Cetina, and Christopher Monroe. Continuous symmetry breaking in a trapped-ion spin chain. *Nature*, 623(7988):713–717, November 2023.

[52] P. Schiffer and I. Daruka. Two-population model for anomalous low-temperature magnetism in geometrically frustrated magnets. *Phys. Rev. B*, 56:13712–13715, Dec 1997.

[53] A. D. LaForge, S. H. Pulido, R. J. Cava, B. C. Chan, and A. P. Ramirez. Quasispin glass in a geometrically frustrated magnet. *Phys. Rev. Lett.*, 110:017203, Jan 2013.

[54] S. V. Syzranov and A. P. Ramirez. Eminuscent phase in frustrated magnets: a challenge to quantum spin liquids. *Nature Communications*, 13(1):2993, may 2022.

[55] Sergey Syzranov. Effect of vacancy defects on geometrically frustrated magnets. *Phys. Rev. B*, 106:L140202, Oct 2022.

[56] Shijun Sun, Arthur P. Ramirez, and Sergey Syzranov. Quasispins of vacancy defects in ising chains with nearest- and next-to-nearest-neighbor interactions. *Phys. Rev. B*, 108:174436, Nov 2023.

[57] Muhammad Sedik, Shijun Sun, Arthur P. Ramirez, and Sergey Syzranov. Quasispins of vacancy defects and their interactions in disordered antiferromagnets. *ArXiv:2404.05845*, 2024.